



<b>GRANT AGREEMENT No.: 764902</b>  <b>Project Acronym: TOMOCON</b>  <b>Project title: Smart tomographic sensors for advanced industrial process control</b>			
<b>Deliverable Rel. No. D4.3.</b>		<b>Lead Beneficiary ULIB</b>	
<b>EU Del. No. D14</b>		<b>Type Report</b>	
<b>WP No. WP4</b>		<b>Date: 15.06.2021</b>	<b>Revision: 0</b>
<b>Innovative Training Network</b>  <b>TOMOCON</b>			
<b>Deliverable Title</b>  <b>Lab-type Integrated Controller Structures for TOMOCON Demonstrations</b>			
<b>Description</b>  <b>This deliverable is a report on the controller structures and their hardware and software implementation for the TOMOCON industrial demonstrations.</b>			

Prepared by:	Dr. Jaroslav Hlava	
Approved by:	Prof. Dr. Uwe Hampel	
Approved by Supervisory Board:	30.06.2021	

Dissemination Level: Public



This project has received funding from the European Union's Horizon 2020 research and innovation programme under the Marie Skłodowska-Curie Grant Agreement No. 764902.

<b>TOMOCON</b>			<b>GRANT AGREEMENT No.: 764902</b>		
Deliverable Title: <b>Lab-type Integrated Controller Structures for TOMOCON Demonstrations</b>					
<b>Del. Rel. No.</b>	<b>EU Del. No.</b>	<b>WP No.</b>	<b>Lead Beneficiary</b>	<b>Type</b>	<b>Date</b>
D4.3.	D14	WP4	ULIB	Report	15.06.2021

### Revision Sheet

<b>Revision Number</b>	<b>Purpose of Revision</b>	<b>Effective Date</b>
0	Initial Issue	30.06.2021



<b>TOMOCON</b>			<b>GRANT AGREEMENT No.: 764902</b>		
Deliverable Title: <b>Lab-type Integrated Controller Structures for TOMOCON Demonstrations</b>					
<b>Del. Rel. No.</b>	<b>EU Del. No.</b>	<b>WP No.</b>	<b>Lead Beneficiary</b>	<b>Type</b>	<b>Date</b>
D4.3.	D14	WP4	ULIB	Report	15.06.2021

## Table of Contents

1.	Introduction .....	5
2.	Demonstration Process: Batch Crystallization .....	6
2.1.	Introduction .....	6
2.2.	Process control and malfunction identification structure .....	6
2.3.	Phase I: The in-line process microscopy system .....	6
2.3.1.	Experimental setup for the in-line process microscopy system .....	7
2.3.2.	PI-based controller implementation.....	8
2.3.3.	LabVIEW program structure for the in-line process microscopy .....	9
2.3.3.1.	Graphical user interface development.....	9
2.3.3.2.	Block diagram development.....	11
2.4.	Phase II: Electrical resistance tomography system.....	14
2.4.1.	Experimental setup for the ERT system.....	15
2.4.2.	ERT-based malfunction diagnostics implementation.....	15
2.4.3.	LabVIEW program structure for ERT .....	16
2.4.4.	Graphical user interface development for ERT .....	17
2.4.4.1.	Block diagram development for ERT .....	18
2.4.5.	Data acquisition and averaging, standard deviation and slope evaluations and decision making.....	19
2.4.6.	LabVIEW State Machines to investigate the malfunction situations .....	20
2.5.	Conclusion .....	24
3.	Demonstration Process: Continuous Casting .....	25
3.1.	Introduction .....	25
3.2.	Control loop.....	26
3.3.	Mini-LIMMCAST setup .....	26
3.4.	Electromagnetic brake.....	28
3.5.	Contactless Inductive Flow Tomography .....	28
3.6.	Controller structure.....	29
3.6.1.	Pre-processing of data.....	29
3.6.2.	Testing.....	29
3.6.3.	Implementation .....	30
4.	Demonstration Process: Inline Swirl Flow Separator .....	33
4.1.	Introduction .....	33
4.2.	System hardware .....	33
4.2.1.	Valve behavior and dynamics .....	34



<b>TOMOCON</b>			<b>GRANT AGREEMENT No.: 764902</b>		
Deliverable Title: <b>Lab-type Integrated Controller Structures for TOMOCON Demonstrations</b>					
<b>Del. Rel. No.</b>	<b>EU Del. No.</b>	<b>WP No.</b>	<b>Lead Beneficiary</b>	<b>Type</b>	<b>Date</b>
D4.3.	D14	WP4	ULIB	Report	15.06.2021

4.2.1.1.	Pressure regulator response.....	34
4.2.1.2.	Valve hysteresis .....	36
4.2.1.3.	Flow coefficient.....	37
4.2.1.4.	Stem dynamics .....	38
4.3.	Control loop and software implementation.....	38
4.3.1.	Operating point and disturbances .....	38
4.3.2.	The controller.....	40
4.3.2.1.	Details on the inverse valve term .....	40
4.3.3.	Controller and observer gains and implementation .....	41
5.	Demonstration Process: Microwave Drying .....	42
5.1.	Introduction .....	42
5.2.	Sensors and control structure.....	42
5.3.	The microwave system and hardware connections .....	43
5.3.1.	Microwave system .....	43
5.3.2.	Control implementation.....	43
5.3.3.	Sensor connections .....	45
5.4.	System identification and control methods .....	46
6.	References.....	48



TOMOCON			GRANT AGREEMENT No.: 764902		
Deliverable Title: <b>Lab-type Integrated Controller Structures for TOMOCON Demonstrations</b>					
Del. Rel. No.	EU Del. No.	WP No.	Lead Beneficiary	Type	Date
D4.3.	D14	WP4	ULIB	Report	15.06.2021

## 1. Introduction

The advantage of using tomographic sensors is that they are able to give us information on what is going on inside the process itself, therefore providing interesting variables that could be controlled. Many processes lack control systems due to the inability of conventional sensors to be implemented. A solution for this is to apply non-invasive sensors such as tomographic sensors to see into the process and obtain useful variables to control. This can then be utilized to design the control loops needed to improve the efficiency of each process. Prospective tomography applications in process control are numerous and although they share certain common features they differ in many aspects.

In this report, we will discuss the controller structure for each of the four demonstrators; we will also review the hardware and software requirements for installing the controllers on the experimental setups. The demonstration processes used in the TOMOCON project are of very different nature and with different control requirements. Hence the report clearly demonstrates that industrial tomography is a very flexible tool in the sense that it can be connected with a wide range of various control approaches.

Batch crystallization control is based on classical PI controller using the stirring speed in the crystallizer as a manipulated variable. Its control and monitoring system was developed in two phases: Phase I which includes the control structure based on the in-line process microscopy system, and Phase II which includes malfunction identification structure based on the ERT system. As for continuous casting, Model Predictive Control (MPC) approach turned out to be the most suitable control solution. It uses jet angle of the flow as a controlled variable which is manipulated by varying the current to the Electromagnetic Brake. Additionally, an algorithm has been developed to obtain the angle of the jet from the reconstructed velocity profile from the CIFT sensors in real time. As similarly done with batch crystallization, the inline swirl flow separator demonstrator control is also based on PI controller that is implemented between the stem position and the core size. The control loop also includes an observer in order to overcome the instability brought to the performance of the separator when acting directly on the sensor output. Lastly, the microwave drying demonstrator has implemented several control approaches. PI controller was implemented to obtain a certain level of moisture distribution inside the material. However, other control approaches have also been investigated including Fuzzy PI, Linear Quadratic Gaussian (LQG), and MPC. Furthermore, control structure includes both feedback and feedforward loops.

As for the software implementation of the controllers, MATLAB/Simulink is used by the continuous casting and microwave drying demonstrators, while LabVIEW is utilized by batch crystallization and inline swirl flow separator demonstrators. The controller programs for all demonstrators are implemented using a Desktop Computer connected to the experimental setups. These approaches to software implementation were selected mainly because of their flexibility and availability of many advanced control and data processing functions. However, in particular in the case of Matlab there is a very straightforward possibility of implementation to dedicated/embedded hardware using the automatic code generation and hardware support functionalities.

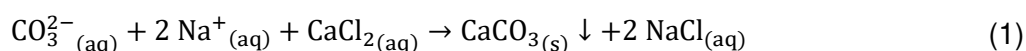


TOMOCON			GRANT AGREEMENT No.: 764902		
Deliverable Title: <b>Lab-type Integrated Controller Structures for TOMOCON Demonstrations</b>					
Del. Rel. No.	EU Del. No.	WP No.	Lead Beneficiary	Type	Date
D4.3.	D14	WP4	ULIB	Report	15.06.2021

## 2. Demonstration Process: Batch Crystallization

### 2.1. Introduction

Real-time characterization and control of fast kinetic crystallization systems have profound importance in ensuring end-product quality and design of these mixing sensitive processes. In the present report, two process monitoring systems are utilized for monitoring and control of a micron-sized, liquid–liquid crystallization process of calcium carbonate ( $\text{CaCO}_3$ ) according to the chemical reaction in Eq. 1:



The instantaneous crystallization process is part of a whole carbon capture and utilization scheme where process control and malfunction diagnostics strategies are presented [1]. The two investigated approaches are as follows:

- Real-time monitoring and control: A commercially available in-line crystallization monitoring system (Pixact Ltd., Finland), which consists of an in situ microscope probe based on refractive index measurement and image analysis by automated edge detection and segmentation procedure.
- Real-time monitoring and malfunction diagnostics: Malfunction detection of the  $\text{CaCO}_3$  crystallization process based on current measurements (microampere,  $\mu\text{A}$ ) from single electrode of an electrical resistance tomography (ERT) system.

### 2.2. Process control and malfunction identification structure

Lab-type integration of controller structures for the batch crystallization process is divided to two phases; Phase I: Control structure based on the in-line process microscopy system, and Phase II: Malfunction identification structure based on the ERT system.

The following sections contain description of hardware, details of software implementation for each phase.

### 2.3. Phase I: The in-line process microscopy system

The Pixact microscopy system is used for in-line monitoring and development of a real-time control framework through a case study involving instantaneous crystallization of calcium carbonate. The utilized backlight-based optical process microscopy probe operates by back illumination from behind the imaged crystals (i.e., transilluminating) and continuously measures the average particle diameter by image analysis technique. Average of the measured micron-sized particles resulting from the reactive crystallization process is used as input to an in-house developed LabVIEW program where a PI controller sends an actuating signal to manipulate the stirring speed in the crystallizer.





TOMOCON			GRANT AGREEMENT No.: 764902		
Deliverable Title: <b>Lab-type Integrated Controller Structures for TOMOCON Demonstrations</b>					
Del. Rel. No.	EU Del. No.	WP No.	Lead Beneficiary	Type	Date
D4.3.	D14	WP4	ULIB	Report	15.06.2021

### 2.3.1. Experimental setup for the in-line process microscopy system

Fig. 1 shows a photograph of the batch-wise calcium carbonate crystallization monitoring and control setup under investigation. The in-line crystallization monitoring system consists of a microscopy probe equipped with high magnification camera, proprietary advanced image analysis software with an industrial computer, and signal generators for control toolbox. The purpose of the signal generator is to convert the scaled mean diameter to an input signal for the feedback control scheme. High-power light source illuminates the measurement head with an optical fiber and a high resolution camera with Gigabit Ethernet (GigE) interface collects blur-free images of the suspension and provides continuous live view from inside the crystallizer.

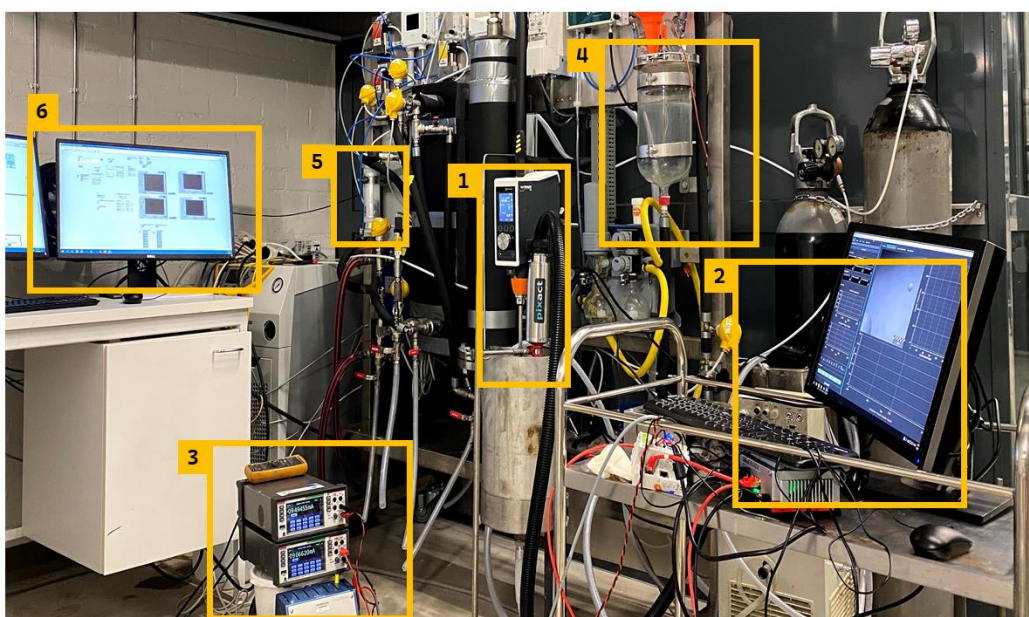


**Fig. 1:** Experimental setup: (1) Pixact crystallization monitoring unit mounted from the top of the stirred tank reactor equipped with a Rushton turbine, (2) Industrial computer for real-time image analysis and monitoring, (3) Milliampere signal conversion via a digital-to-analog converter for the control system, (4) Glass vessel that contains NaOH absorbent liquid for CO<sub>2</sub> capture, (5) Commercial-grade hollow fiber membrane as the gas-liquid contactor, (6) Computer for process control with LabVIEW software.

The experimental setup consists of a stainless-steel baffled crystallizer of 220 diameter mm (height/diameter = 1.6) equipped with an overhead stirrer (Heidolph Instruments GmbH). The mixing speed of a standard six-blade Rushton turbine (diameter = 88 mm) varies in the range of 50 RPM (0.83 rps very low) to 300 RPM (5 rps, maximum). In the crystallization system, aqueous CO<sub>3</sub><sup>2-</sup> as the reagent solution flows through an inlet pipe (diameter: 2 mm) into the crystallizer containing calcium chloride.

TOMOCON			GRANT AGREEMENT No.: 764902		
Deliverable Title: <b>Lab-type Integrated Controller Structures for TOMOCON Demonstrations</b>					
Del. Rel. No.	EU Del. No.	WP No.	Lead Beneficiary	Type	Date
D4.3.	D14	WP4	ULIB	Report	15.06.2021

### 2.3.2. PI-based controller implementation

The kinetics of the ionic-based reactive crystallization processes are in general fast, nonlinear and complex, rendering them difficult to control [2]. In fast kinetic systems, mixing at meso-scale becomes a dominant factor and has a significant impact on process characteristics such as crystal size distribution and shape [3,4]. Given the sensitivity of these processes to hydrodynamics condition in the reactor, a traditional proportional-integral (PI) controller to manipulate the supersaturation dispersion and agitation intensity according to an in situ real-time measurement of the mean particle size can enable a robust direct design in fast-reaction crystallization processes [5,6]. A closed-loop (feedback) control system, adjusts the control variable (e.g., mixing speed) according to a pre-defined set-point of a key process parameter (e.g., average diameter).

The output of a PID algorithm is expressed by the composition of three different correcting terms [7]:

$$u(t) = K_p e(t) + K_i \int_{t_0}^t e(\zeta) d\zeta + K_d \dot{e}(t) \quad (2)$$

Where  $u$  is the controller output (e.g., mixing speed),  $e$  is the error between the set-point and the measured output,  $K_p$ ,  $K_i$ ,  $K_d$  are the positive gains for proportional, integral and derivative terms, respectively;  $\zeta$  denotes the integration variable, representing the time elapsed since the initial time  $t_0$ .

In the present study, a PI controller is implemented in the LabVIEW software (National Instruments) where the output signal of the controller is the impeller rotation speed (i.e., manipulated variable). PI controller lacks the derivative action of a PID system and has been widely applied in process industries [8,9].

Two adjustable parameters of the PI controller can provide satisfactory performance for basic applications and detailed mathematical knowledge of the process is not necessarily needed for tuning the gain parameters. Controller gains can be manually adjusted by trial and error procedures according to the stability and transient response (overshoot, rising time, and settling time) of the system under investigation [10]. The PI algorithm considerably decreases the offset (i.e., deviation from the set-point), however, a key inherent limitation is the relative slow response time [11]. The latter one can be significantly improved by applying delay compensation algorithms [12].

The schematics in Fig. 2 present the structural design of the image analysis-based reactive crystallization control. A feedback connection is established by acquiring the milliampere signals of the in-line microscopy probe. A digital-to-analog converter (Keithley DMM6500 6) is used for signal conversion and transformation.

Particle diameter data are stored in a temporary data storage layer (buffer layer) and then averaged over a specific, user-controlled sample length. Real-time adjustment of the





TOMOCON			GRANT AGREEMENT No.: 764902		
Deliverable Title: <b>Lab-type Integrated Controller Structures for TOMOCON Demonstrations</b>					
Del. Rel. No.	EU Del. No.	WP No.	Lead Beneficiary	Type	Date
D4.3.	D14	WP4	ULIB	Report	15.06.2021

sampling length and intervals allow a rational approximation of the transient distribution of particle sizes in the stirred tank reactor. In case of a difference between the set-point diameter of the controller and the incoming signal from the in situ probe, an actuating signal is applied on the manipulated variable within the next operational loop of the process. An experimental correlation between the mixing speed and the mean particle size is used as the PI controller logic.

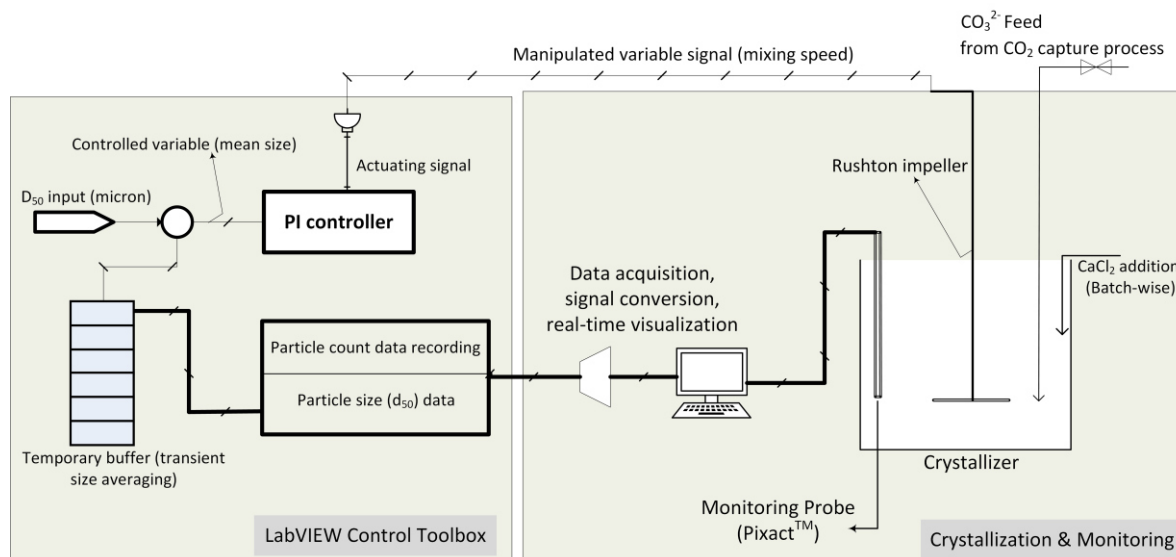


**Fig. 2:** Schematic representation of the experimental setup and structural design of the image analysis-based PI controller during calcium carbonate reactive crystallization process

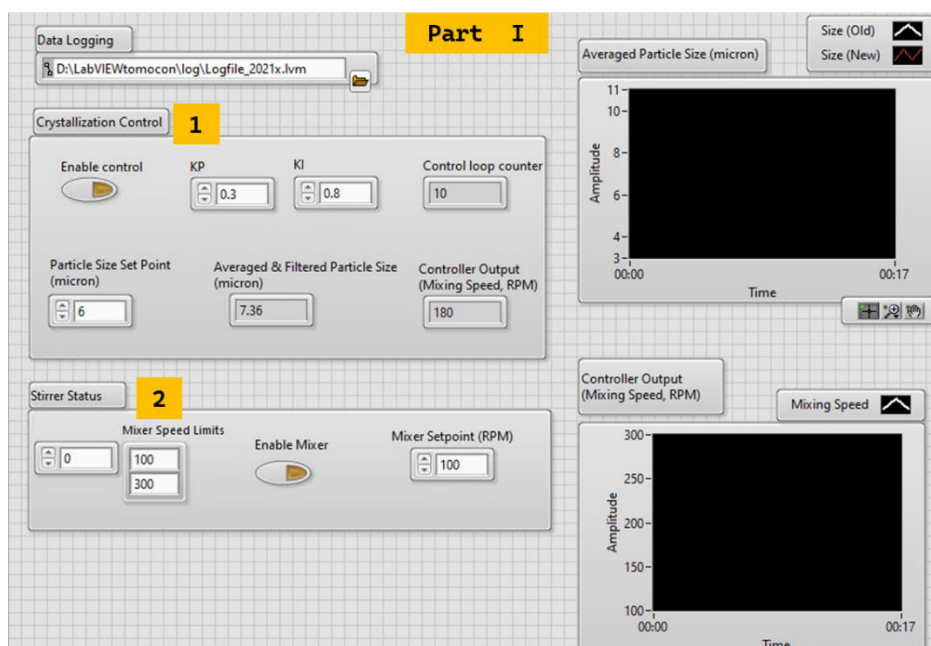
### 2.3.3. LabVIEW program structure for the in-line process microscopy

An image analysis-based feedback control program is implemented in the LabVIEW software based on the results of the open-loop experiments and the sensitivity of the crystallization process to hydrodynamics condition in the stirred tank reactor. A set-point tracking PI controller enables the manipulation of the agitation intensity in the crystallizer and maintains a target crystal property with a reasonable accuracy. The accuracy of the entire process control and the reproducibility for each batch operation is assessed based on using the standard deviation of the final mean crystal size and distribution width (span) in open-loop and closed loop experiments.

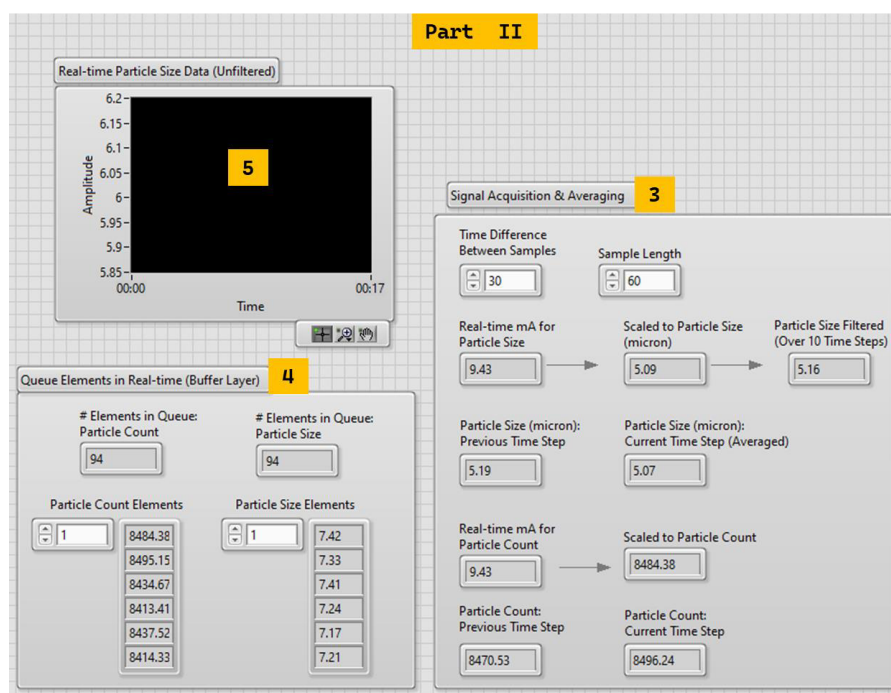
#### 2.3.3.1. Graphical user interface development

Fig. 3 and Fig. 4 show an overview of the graphical user interface (GUI) of the LabVIEW program. The program allows a user to monitor the real-time development of the crystallization process and in case needed, appropriate actions can be applied. For instance, tuning gain parameters, sampling length and time intervals for particle size averaging and mixing speed limits can be specified online according to the evolution of the experiment.

<b>TOMOCON</b>				<b>GRANT AGREEMENT No.: 764902</b>	
Deliverable Title: <b>Lab-type Integrated Controller Structures for TOMOCON Demonstrations</b>					
<b>Del. Rel. No.</b>	<b>EU Del. No.</b>	<b>WP No.</b>	<b>Lead Beneficiary</b>	<b>Type</b>	<b>Date</b>
D4.3.	D14	WP4	ULIB	Report	15.06.2021



**Fig. 3:** Graphical user interface of the LabVIEW program for real-time reactive crystallization control, Part I



**Fig. 4:** Graphical user interface of the LabVIEW program for real-time reactive crystallization control, Part II

The main parts of the program are as follows (numbers are displayed in Fig. 3 and 4):

1. Crystallization Control: Process control is activated, and particle size set-point value is defined.



TOMOCON				GRANT AGREEMENT No.: 764902	
Deliverable Title: <b>Lab-type Integrated Controller Structures for TOMOCON Demonstrations</b>					
Del. Rel. No.	EU Del. No.	WP No.	Lead Beneficiary	Type	Date
D4.3.	D14	WP4	ULIB	Report	15.06.2021

2. Stirrer Status: Switching on/off of the stirrer, lower and upper boundaries of the mixing are applied and can be manipulated.
3. Signal Acquisition and Averaging: Sampling length and time difference between samples can be defined via the numeric controls and indicators. Also, additional information about particle size and count are displayed in real-time.
4. Queue Elements in Real-time (Buffer Layer): The buffer layer acts as a temporary data storage layer and stores the particle size and count in arrays. Transient size averaging is performed based on a user-controlled sample length and obtains the data from buffer layer.
5. Monitoring plots and graphs: Plots show the real-time data acquisition (filtered and unfiltered particle size,  $\mu\text{m}$ ) and the controller output (mixing speed, RPM).

### 2.3.3.2. Block diagram development

The implemented source code of the LabVIEW-based crystallization control is developed in 4 main block diagrams, namely:

- I. mA Signal Acquisition & Conversion to Particle Count
- II. mA Signal Acquisition & Conversion to Particle Size
- III. Mixer Control Loop
- IV. Signal Averaging, Set Point & PI Controller

The overall structure of the block diagrams are described in the following sections.

Fig. 5 shows the block diagram “I: mA Signal Acquisition & Conversion to Particle Count”. The LabVIEW program reads the current (mA) from the measurement system each 1000 milliseconds (ms) and a function scales the current measurements to particle count. The particle count scaling function is tuned by trial and error, which depends on the specifications of the measurement equipment and the approximation of the maximum particle number per image. Particle size scaling and signal acquisition within the block, “II. mA Signal Acquisition & Conversion to Particle Size”, is performed in a similar fashion, which is presented in Fig. 6.



TOMOCON			GRANT AGREEMENT No.: 764902		
Deliverable Title: <b>Lab-type Integrated Controller Structures for TOMOCON Demonstrations</b>					
Del. Rel. No.	EU Del. No.	WP No.	Lead Beneficiary	Type	Date
D4.3.	D14	WP4	ULIB	Report	15.06.2021

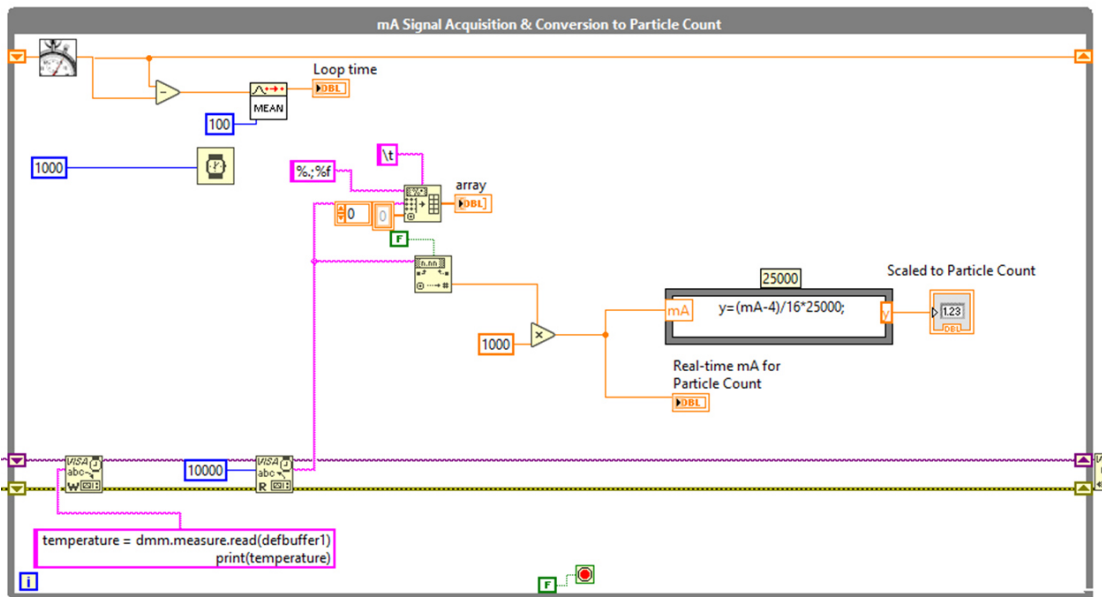


**Fig. 5:** Block diagram for signal acquisition from the measurement probe and conversion to particle count

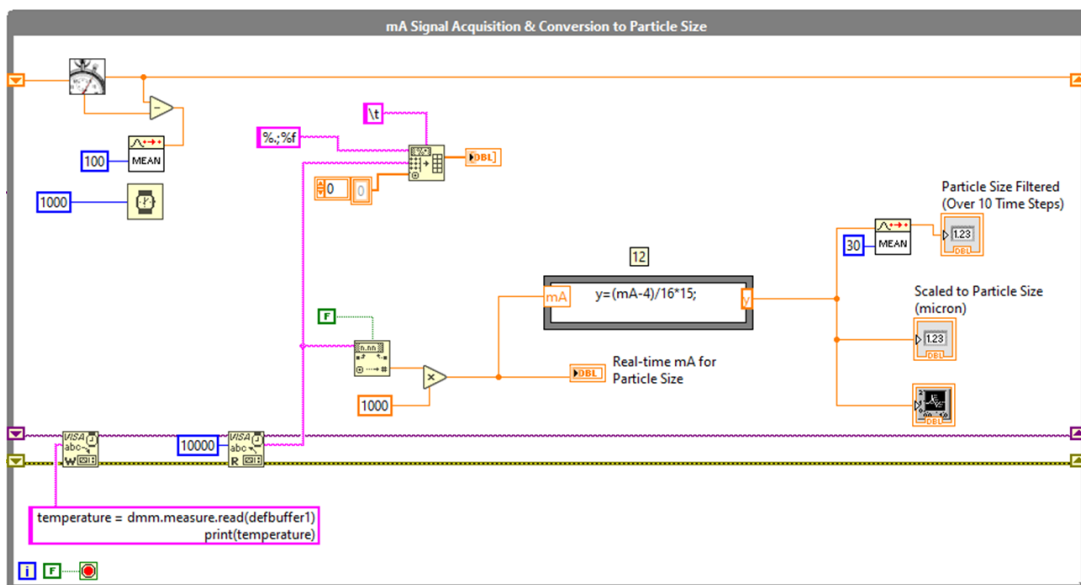


**Fig. 6:** Block diagram for signal acquisition from the in-line probe and conversion to particle size

Block diagram “III: Mixer Control Loop” is implemented by establishing a direct connection between the mixer and the LabVIEW via a USB interface cable. A series of LabVIEW State Machines are defined for mixer manipulation. State Machines are used to define a clear number of states and subsequent events (e.g., mixer on/off, waiting mode, etc.). Fig. 7 displays a snapshot of the Mixer Control Loop while the state “Run” is selected.



Deliverable Title: **Lab-type Integrated Controller Structures for TOMOCON Demonstrations**

Del. Rel. No.	EU Del. No.	WP No.	Lead Beneficiary	Type	Date
D4.3.	D14	WP4	ULIB	Report	15.06.2021

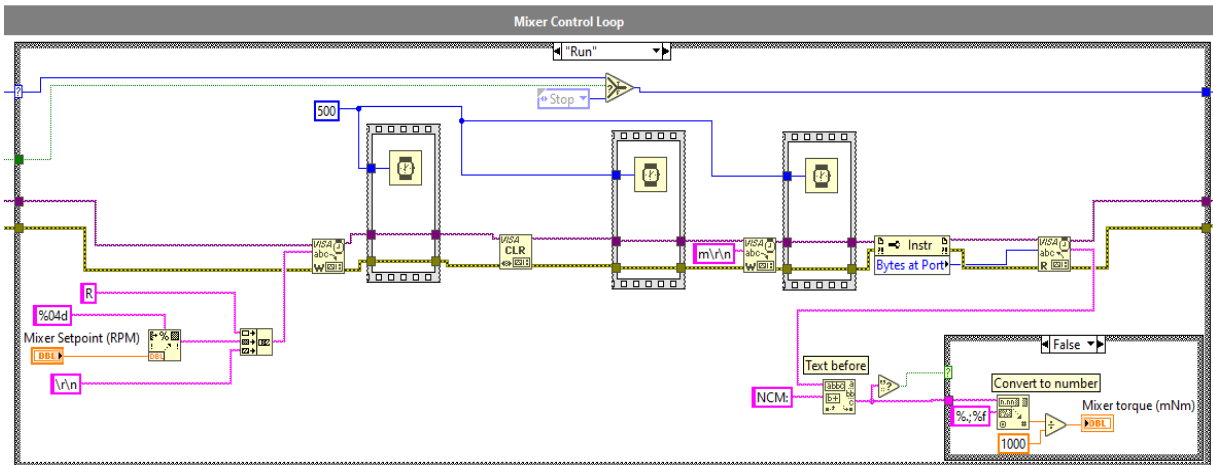


**Fig. 7:** LabVIEW block diagram for mixing control. Establishing a connection between the mixer and the program is done by a USB cable

Block diagram “IV: Signal Averaging, Set Point & PI Controller” consists of an array formation from the scaled signals, defining the averaging schemes and a PI controller. Each of the particle count and size parameters form an array and a series of mean functions evaluate the average value based on the parameters “Sample Length” and “Time Difference Between Samples”. “Sample Length” corresponds to the array index and is a user-defined value that specifies the number of elements that can be used for averaging. Since data acquisition is performed each 1000 ms, thus each row in the arrays corresponds to 1 s. The parameters “Time Difference Between Samples” conducts the same operation with a user-defined time delay. Fig. 8 shows a snapshot of the array formation and averaging procedures.

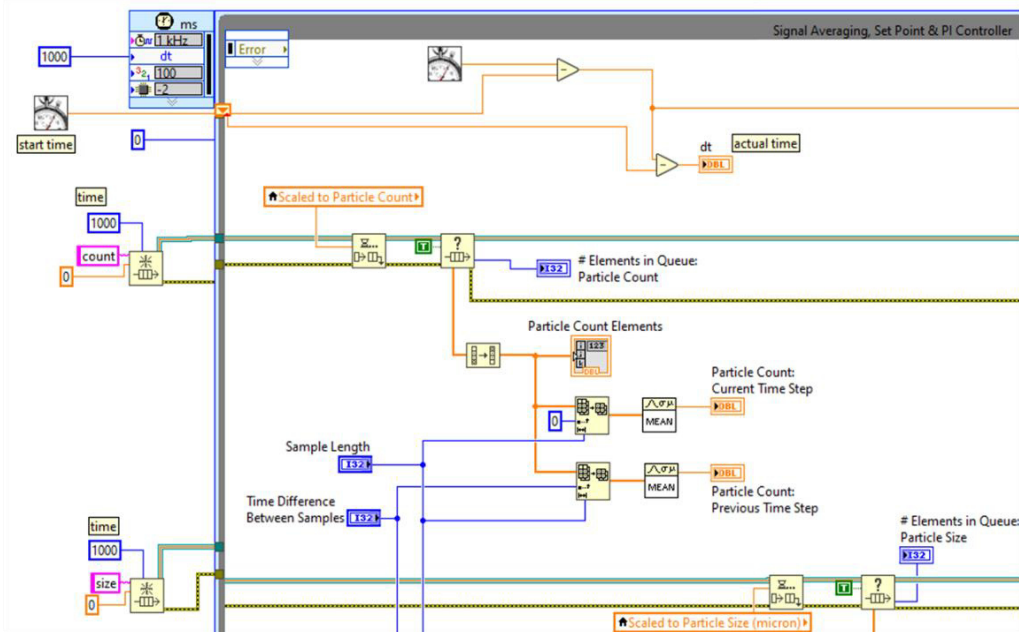


**Fig. 8:** LabVIEW block diagram representing signal acquisition, array formation and averaging procedures



TOMOCON				GRANT AGREEMENT No.: 764902	
Deliverable Title: Lab-type Integrated Controller Structures for TOMOCON Demonstrations					
Del. Rel. No.	EU Del. No.	WP No.	Lead Beneficiary	Type	Date
D4.3.	D14	WP4	ULIB	Report	15.06.2021

The averaged particle size (micron) is filtered and then used as the input to the PI controller (Fig. 9). The experimental correlation is used as the main logic of the controller: Increase in intensity of the agitation at a constant feed addition rate, results in a relative increase in average crystal size and vice versa. In order to develop the set point tracking PI controller framework, the volumetric feed flow rate is constant for each operating condition, thus variation in the crystal size is only due to the hydrodynamics condition in the crystallizer. In the present work, input values of  $K_p$  and  $K_I$  are estimated by trial and error procedure and kept constant at 0.3 and 0.8, respectively. Value of zero is assigned to  $K_d$ .

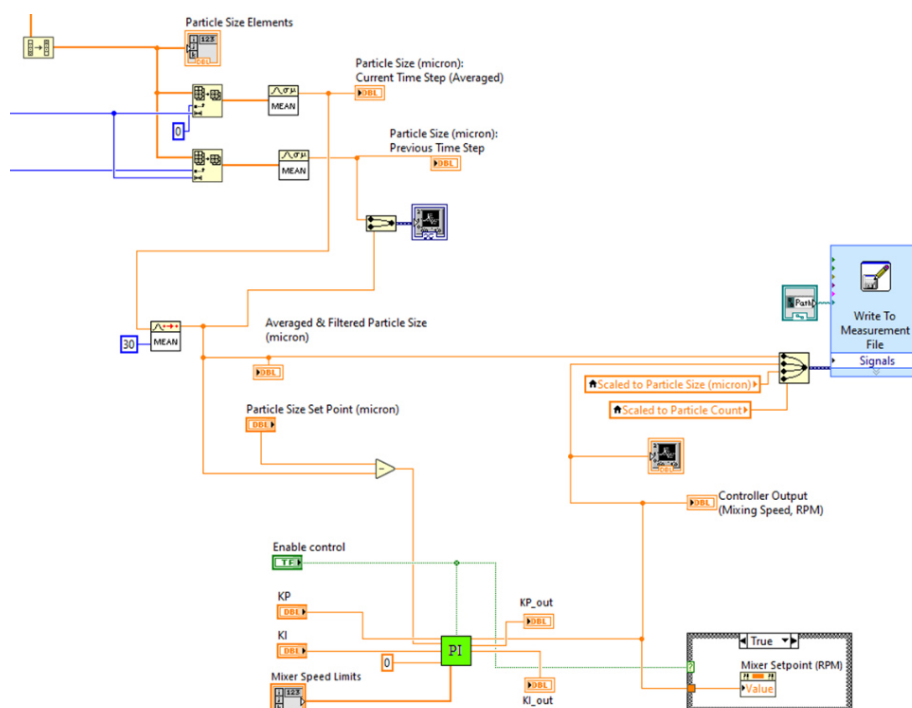


**Fig. 9:** LabVIEW block diagram for developing the feedback controller based on the in-line measurement probe signals

## 2.4. Phase II: Electrical resistance tomography system

The utilized electrical resistance tomography is based on injection of a constant electrical voltage and simultaneously measuring the electrical field distribution. The crystallization reactor is equipped with a single row of 16 stainless steel electrodes mounted around the perimeter. The frequency of operation is 156 KHz and image capturing frame rate is 14.7 Hz. A modified Bayesian method is utilized for image reconstruction. A detailed description of the ERT system is provided in TOMOCON Deliverable No. 2.4 and in [13,14].

In addition to image reconstruction, single- and multi-electrode current measurements from the ERT system can be exploited for real-time fault detection, quality assurance and malfunction diagnosis when out-of-specification events occur throughout the entire process.





TOMOCON			GRANT AGREEMENT No.: 764902		
Deliverable Title: <b>Lab-type Integrated Controller Structures for TOMOCON Demonstrations</b>					
Del. Rel. No.	EU Del. No.	WP No.	Lead Beneficiary	Type	Date
D4.3.	D14	WP4	ULIB	Report	15.06.2021

A LabVIEW program is developed to investigate the feasibility of the fault detection and diagnostics (FDD) during the  $\text{CaCO}_3$  reactive crystallization process.

### 2.4.1. Experimental setup for the ERT system

Fig. 10 shows a photograph of the entire experimental setup in which the ERT system is utilized for the FDD analysis. The crystallization reactor is made of plexiglass with an inner diameter of 190 mm. In the crystallization system, aqueous  $\text{CO}_3^{2-}$  as the reagent solution flows through an inlet pipe (diameter: 2 mm) into the crystallizer containing calcium chloride.

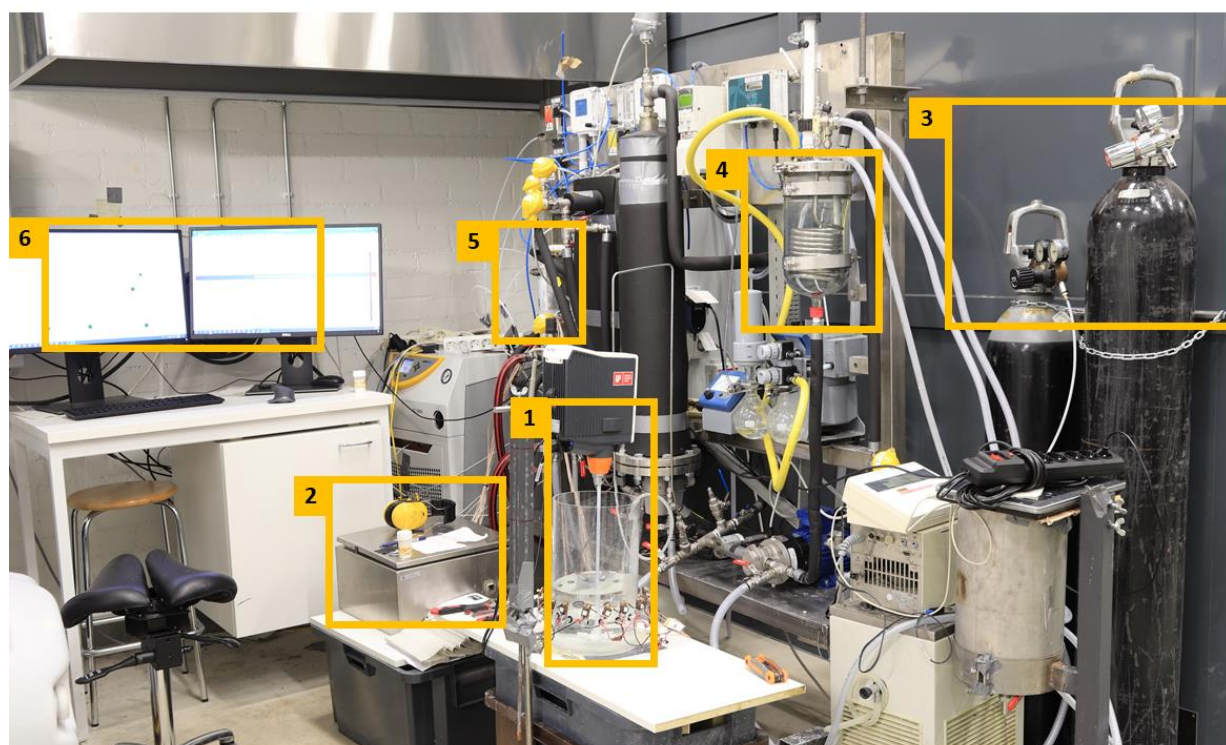


**Fig. 10:** (1) Electrical Resistance Tomography unit mounted around a stirred tank reactor equipped with a Rushton turbine, (2) Electronics for data acquisition and connection to computer via Ethernet cable, (3) Air/ $\text{N}_2$  and  $\text{CO}_2$  bottles, (4) Glass vessel that contains absorbent liquid (NaOH) for  $\text{CO}_2$  capture, (5) Commercial-grade hollow fiber membrane as the gas-liquid contactor, (6) Computer for process monitoring with LabVIEW software.

### 2.4.2. ERT-based malfunction diagnostics implementation

The integrated crystallization- $\text{CO}_2$  capture of the present study consists of several key physical and chemical components such as feeding pump, mixer, reagent solution,  $\text{CO}_2$  gas absorbent solution concentration and amount of calcium chloride in the receiving reactor. Occurrence of unfavorable faults and malfunctions in the process stream, negatively impacts the final product, and results in a crystallization failure.

<b>TOMOCON</b>			<b>GRANT AGREEMENT No.: 764902</b>		
Deliverable Title: <b>Lab-type Integrated Controller Structures for TOMOCON Demonstrations</b>					
<b>Del. Rel. No.</b>	<b>EU Del. No.</b>	<b>WP No.</b>	<b>Lead Beneficiary</b>	<b>Type</b>	<b>Date</b>
D4.3.	D14	WP4	ULIB	Report	15.06.2021

Electrical resistance tomography measurements and real-time statistical analysis of the signals are used as a mean for fault detection, and in case needed, prompt actions can be taken to restore the affected equipment. Because there is a relatively large theoretical combination of such faults, the investigated cases in the present work represent the ones with practical interest to the entire process. The fault tree analysis (FTA) methodology is used to develop the system failure modes irrespective of their severity.

Different scenarios of the ERT-based malfunction investigation are tabulated in Table 1. Currently, only single electrode of the ERT is used to develop the program and to conduct the experiments. The selected electrode is located relatively close to the feed point, which increases the sensitivity and has shown stable and consistent measurement during the experimental repetition process.

**Table 1.** Different fault detection and diagnostics scenarios investigated with ERT system

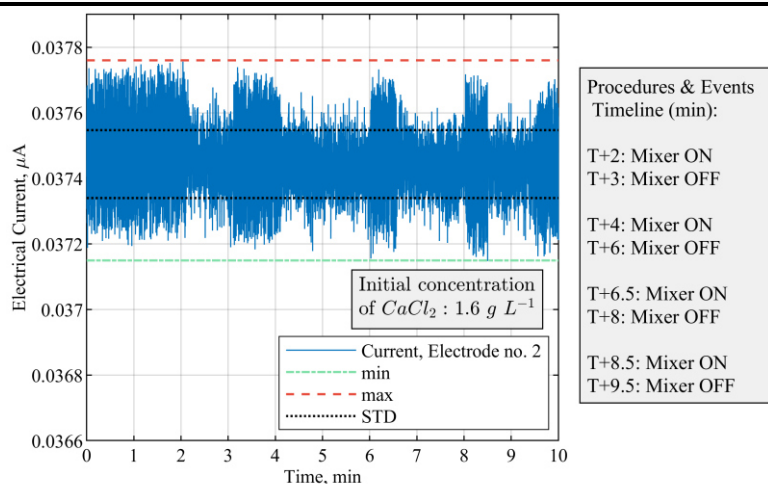
	<b>Constantly Operational</b>	<b>Malfunction during the process</b>
<b>Case no. 1</b>	Pump ON	Mixer OFF
<b>Case no. 2</b>	Mixer ON	Pump ON/OFF
<b>Case no. 3</b>	—	Mixer ON & OFF, Pump ON & OFF
<b>Case no. 4</b>	Pump ON, Mixer ON	Calcium Chloride consumed
<b>Case no. 5</b>	Pump ON, Mixer ON	Feed is water (not carbonate ions)

### 2.4.3. LabVIEW program structure for ERT

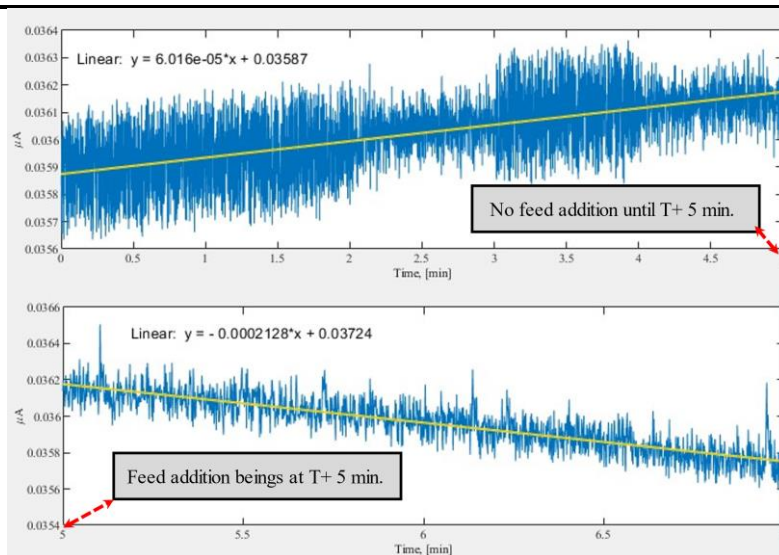
Single-electrode measurements are sensitive to the real-time events during the crystallization process. For instance, there is a salient contrast in the acquired signals when the mixer is switched on or switched off. In a similar fashion, when the feed addition is working properly or it has concentration issues, the patterns in the signals are different. The former one (i.e., mixing) affects the standard deviation (or amplitude) of the signals (Fig. 11a), while the latter one affects the slope (Fig. 11b). Hence, the ERT-based malfunction investigation with LabVIEW integration is developed based on the existing patterns in the signals, dynamic data analysis procedures and performing a comprehensive total ion balance calculation of the entire chemical process.



<b>TOMOCON</b>				<b>GRANT AGREEMENT No.: 764902</b>	
Deliverable Title: <b>Lab-type Integrated Controller Structures for TOMOCON Demonstrations</b>					
<b>Del. Rel. No.</b>	<b>EU Del. No.</b>	<b>WP No.</b>	<b>Lead Beneficiary</b>	<b>Type</b>	<b>Date</b>
D4.3.	D14	WP4	ULIB	Report	15.06.2021



(a)



(b)

**Fig. 11:** Dynamic data analysis and patterns of the ERT single-electrode measurement. (a): Effects of mixing on ERT measurements; (b): Effects of feed addition on ERT measurement during the crystallization process.

The following sections contain a description of the graphical user interface and block diagrams of the LabVIEW program.

#### 2.4.4. Graphical user interface development for ERT

The LabVIEW program reads the ERT measurements in real-time and utilizes the information of the electrode number 2 to perform the analysis. As displayed in Fig. 12, the GUI of the LabVIEW program consists of 6 main components:



TOMOCON			GRANT AGREEMENT No.: 764902		
Deliverable Title: <b>Lab-type Integrated Controller Structures for TOMOCON Demonstrations</b>					
<b>Del. Rel. No.</b>	<b>EU Del. No.</b>	<b>WP No.</b>	<b>Lead Beneficiary</b>	<b>Type</b>	<b>Date</b>
D4.3.	D14	WP4	ULIB	Report	15.06.2021

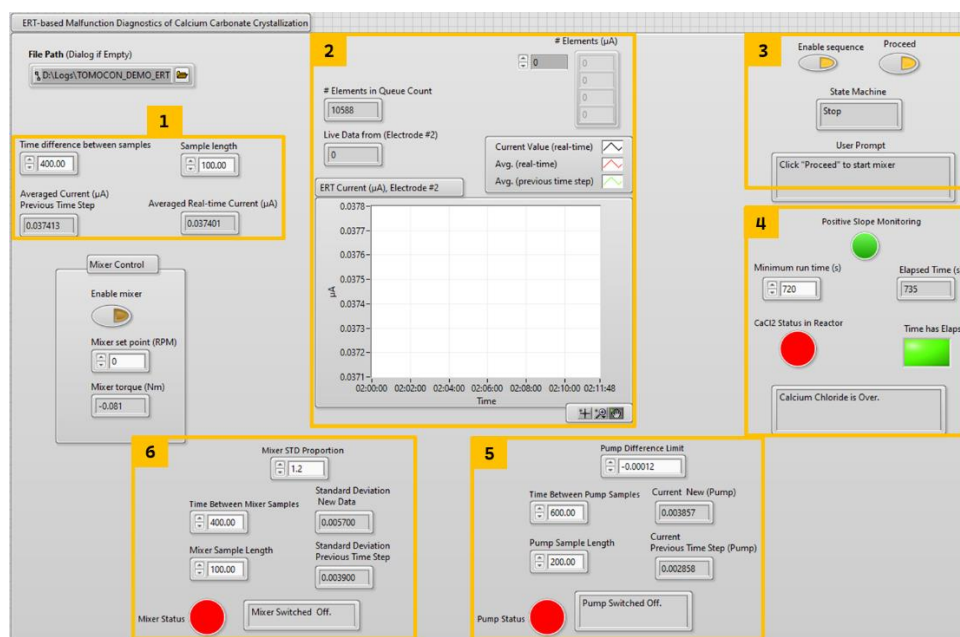


**Fig. 12:** GUI of the LabVIEW program for real-time calcium carbonate crystallization monitoring, fault detection and malfunction identification

1. ERT measurements sampling and averaging over user-defined sample length. LabVIEW data acquisition rate is set at 50 ms.
2. ERT data (averaged, filtered, and non-filtered) are plotted for real-time visualization.
3. ERT-based process automation and fault detection begins by implementing a series of LabVIEW State Machines.
4. Minimum run time of the crystallization process is defined by carrying out a total ion balance calculation for the entire chemical process. Ionic balance information is used to make decisions on the calcium chloride status in the reactor. Also, crystallization termination command (i.e., switching off mixer and feed pump) is performed automatically when the measured slope is positive, and the minimum run time has elapsed.
5. Fault detection for pump is determined based on the descending slope of the real-time signals. The incoming carbonate ions reacts with the pre-existing calcium chloride and leads to a relative reduction in conductivity field of the medium (Fig. 11b).
6. Stirrer fault detection is determined by a significant variation in standard deviation of the incoming conductivity signals (Fig. 11a). A relative increase in the averaged standard deviation represents a situation where the mixer is switched off and a red-color alert appears on the GUI (Fig. 12).

#### 2.4.4.1. Block diagram development for ERT

Block diagram for the LabVIEW-based crystallization fault detection is developed in 2 parts as described in the following sections.





TOMOCON				GRANT AGREEMENT No.: 764902	
Deliverable Title: <b>Lab-type Integrated Controller Structures for TOMOCON Demonstrations</b>					
Del. Rel. No.	EU Del. No.	WP No.	Lead Beneficiary	Type	Date
D4.3.	D14	WP4	ULIB	Report	15.06.2021

### 2.4.5. Data acquisition and averaging, standard deviation and slope evaluations and decision making

Fig. 13 shows the block diagrams related to “Calcium Chloride Status” in the reactor. Incoming ERT measurements with a data acquisition rate of 50 ms is stored in arrays. The parameter “Averaged Real-time Current (µA)” determines the current value (µA) based on a “Sample length”. Averaged ERT current from previous times steps is evaluated at the same time. If the newly-measured currents are greater than the previous time steps, a red-color alert is switched on, which indicates an ascending slope. The process is terminated *if and only if* the slope is continuously positive and the pre-defined minimum run time has elapsed.

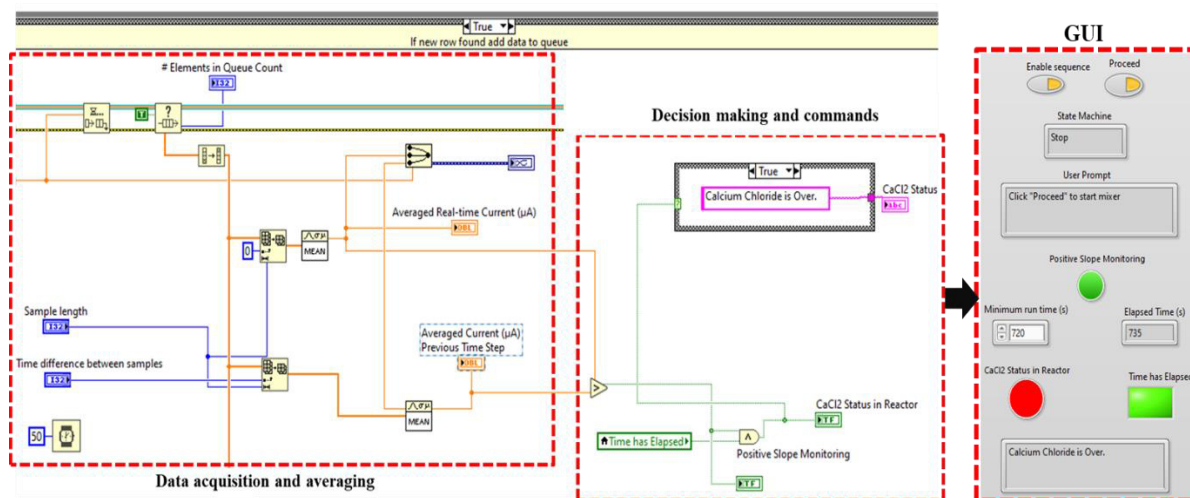


**Fig. 13:** Block diagrams to identify the status of the calcium chloride in the reactor and automatic process termination based on minimum run time

Standard deviation and slope of the ERT measurements are utilized in order to determine the mixing and pump status, respectively. Fig. 14 shows the block diagram of the procedure and the subsequent GUI.

If the evaluated standard deviation (SD) is greater than a given parameter known as “Mixer STD Proportion”, then it indicates a situation where the mixer is switched off (Fig. 11a). The mixer SD ratio is obtained through experimental data based on the following relation:

$$\text{Mixer SD Ratio} = \frac{\text{signal SD when mixer is switched on}}{\text{signal SD when mixer is switched off}} \quad (3)$$

Block diagrams to determine the pump status follows a similar pattern by calculating and comparing the newly measured slope to the previous sampling time.



TOMOCON			GRANT AGREEMENT No.: 764902		
Deliverable Title: <b>Lab-type Integrated Controller Structures for TOMOCON Demonstrations</b>					
Del. Rel. No.	EU Del. No.	WP No.	Lead Beneficiary	Type	Date
D4.3.	D14	WP4	ULIB	Report	15.06.2021

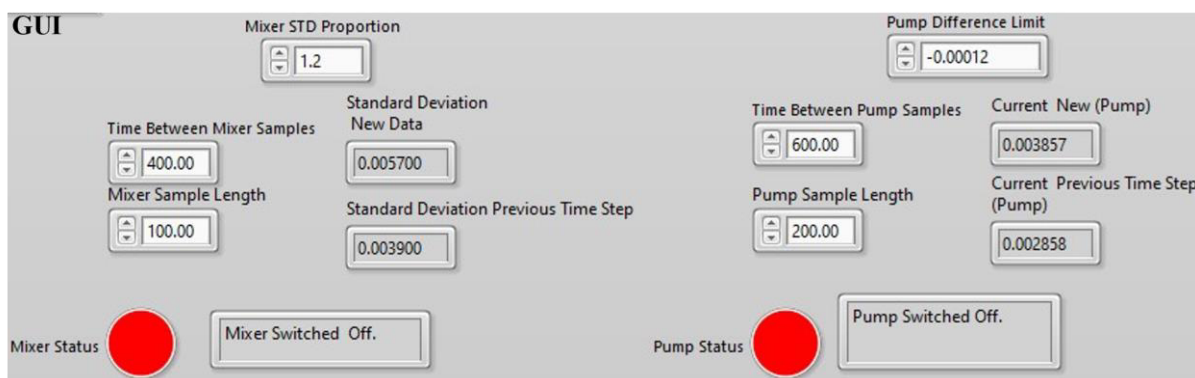
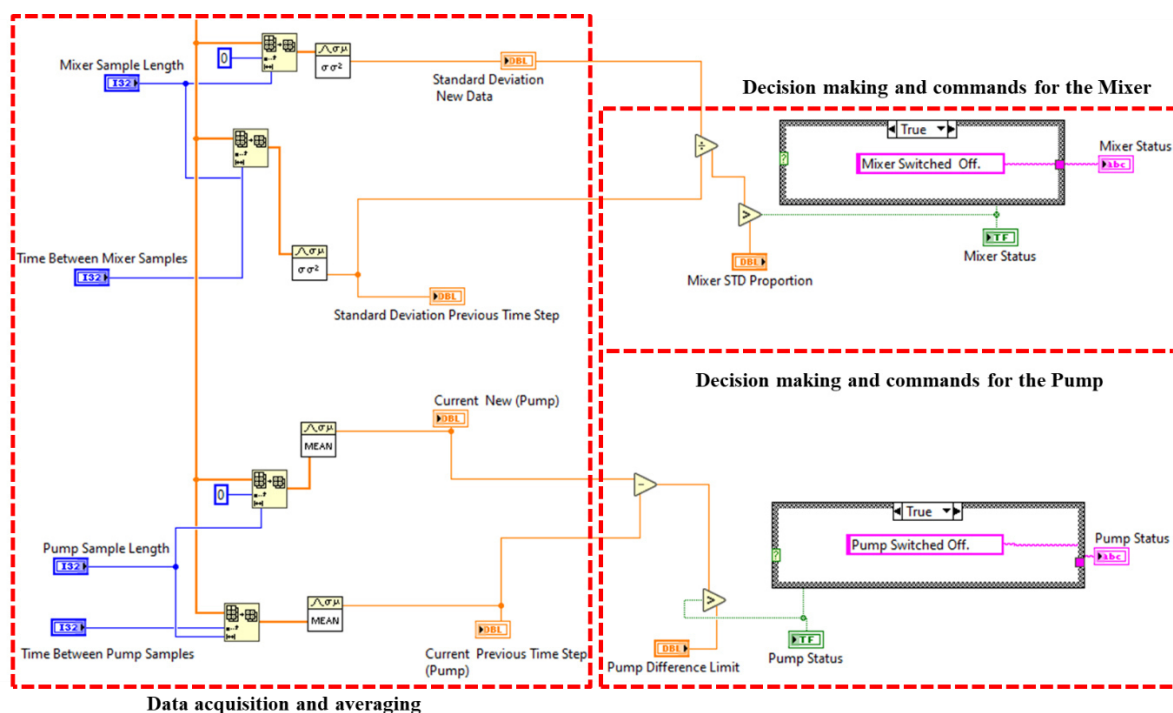


**Fig. 14:** Block diagram and the resulting GUI to identify mixing and pump (feed addition) malfunctions during the crystallization process

#### 2.4.6. LabVIEW State Machines to investigate the malfunction situations

Triggering each state is based on user commands and also process automation. States are defined to enhance the process automation and investigate different malfunction scenarios (Table 1). A description of 5 different states and the block diagram are discussed in the following section.



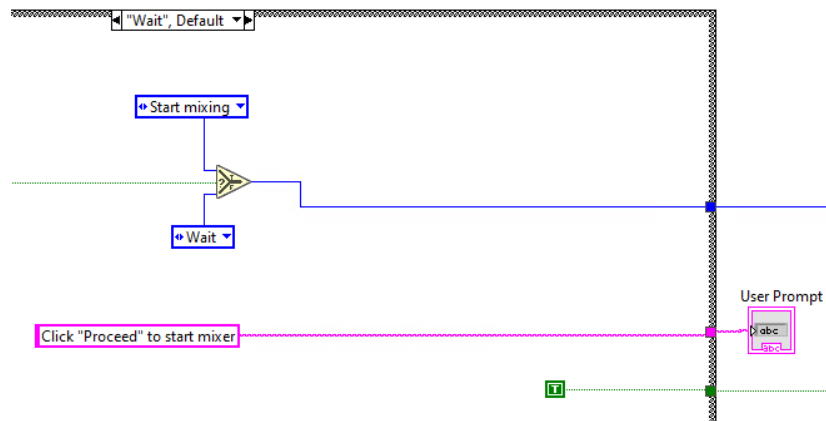


TOMOCON			GRANT AGREEMENT No.: 764902		
Deliverable Title: <b>Lab-type Integrated Controller Structures for TOMOCON Demonstrations</b>					
Del. Rel. No.	EU Del. No.	WP No.	Lead Beneficiary	Type	Date
D4.3.	D14	WP4	ULIB	Report	15.06.2021

### STATE 1: Wait Mode

#### Process Automation Startup

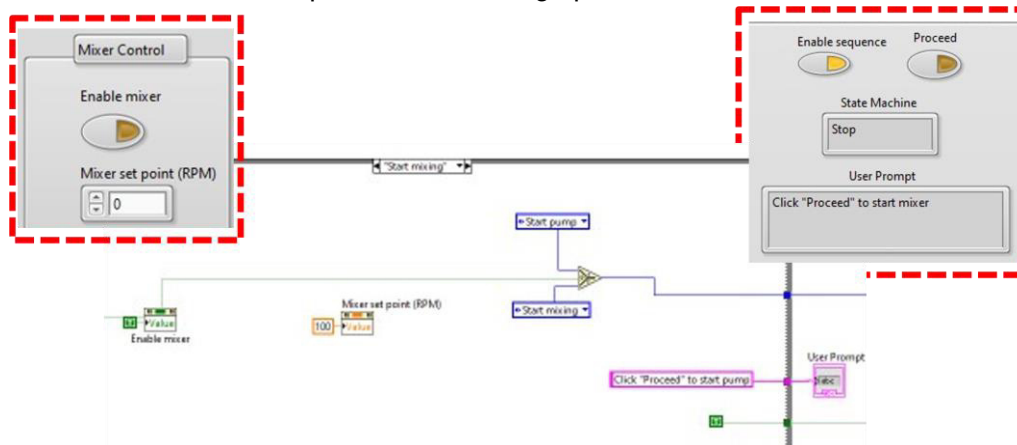
By activating the “enable sequence” button on the GUI, the program shifts to the Wait Mode. Experiment has not yet started at this phase and both the mixer and feed addition are off.



### STATE 2: Mixing Starts

#### Automatic Mixing Activation:

If the entire system is ready (user decision), by pressing the “proceed” button on the GUI, mixing SWITCHES-ON with a pre-defined mixing speed.

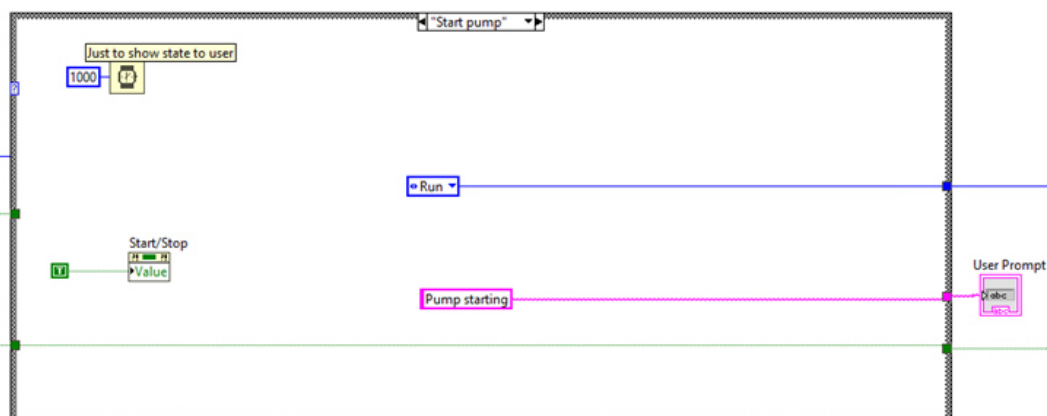


TOMOCON				GRANT AGREEMENT No.: 764902	
Deliverable Title: <b>Lab-type Integrated Controller Structures for TOMOCON Demonstrations</b>					
Del. Rel. No.	EU Del. No.	WP No.	Lead Beneficiary	Type	Date
D4.3.	D14	WP4	ULIB	Report	15.06.2021

### STATE 3: Pump Starts

#### Automatic Pump Activation:

If mixing is SWITCHED-ON and the overall system is OK (user decision), then the feed (pump) gets SWITCHED-ON. At this time, the experiment is ongoing and the “Elapsed Time (s)” on the GUI is activated.



### STATE 4: Experiment is Running

#### Experiment is Ongoing:

##### Mixing:

If malfunction does not happen during the experiment, mixing maintains the SWITCHED-ON state during the crystallization. Crystallization duration is defined based on the theoretical ion balance for the individual experiment. Moreover, mixing follows the pump state only after reaching to the ion balance level (i.e., pump gets off, then mixer gets off).

##### Pump:

- Pump state is monitored based on the continuous ERT measurement. If malfunction does not happen during the experiment, pump maintains the SWITCHED-ON mode until reaching the minimum theoretical ion balance level.





TOMOCON			GRANT AGREEMENT No.: 764902		
Deliverable Title: <b>Lab-type Integrated Controller Structures for TOMOCON Demonstrations</b>					
Del. Rel. No.	EU Del. No.	WP No.	Lead Beneficiary	Type	Date
D4.3.	D14	WP4	ULIB	Report	15.06.2021

## 2.5. Conclusion

The present report demonstrates the applicability of two process monitoring tools for real-time calcium carbonate reactive crystallization control, fault detection and diagnostics (FDD).

A LabVIEW-based program is developed for the crystallization monitoring and control with an in-line process microscopy probe. The in-line probe operates at its maximum resolution due to micron-range crystals, and utilizes digital image processing coupled with advanced recognition of solid particle boundaries to analyse the crystallization process.

Additionally, single-electrode measurements from an electrical resistance tomography system is exploited to develop a LabVIEW program for automatic crystallization malfunction identification and fault detection. ERT-based FDD analysis is based on total ion balance of the entire chemical process and dynamic statistical analysis of the measured current (microampere,  $\mu\text{A}$ ) from single electrode. Different scenarios for mixing, pump and concentration malfunction are investigated. Mixing status identification is developed by dynamic standard deviation analysis, while the current slope analysis is used for reporting the pump (feed addition) situation.



TOMOCON				GRANT AGREEMENT No.: 764902	
Deliverable Title: <b>Lab-type Integrated Controller Structures for TOMOCON Demonstrations</b>					
Del. Rel. No.	EU Del. No.	WP No.	Lead Beneficiary	Type	Date
D4.3.	D14	WP4	ULIB	Report	15.06.2021

### 3. Demonstration Process: Continuous Casting

#### 3.1. Introduction

Continuous casting is an important process that is used to produce about 95% of the world’s steel production. The principal operation of a continuous caster is shown in Fig. 15. Liquid steel or other metal flows from the ladle to the tundish and from there via a submerged entry nozzle (SEN) into the mould. The flow rate there is controlled by a stopper rod or a sliding gate. In the water-cooled mould a solid steel shell is formed, and the partly solidified strand is further transported on rolls and cooled by water sprays until it is solidified completely. The quality of the final product is closely related to the flow regime in the SEN and in the mould. Unstable flows in the mould can lead to surface defects or slag entrapment. Electromagnetic actuators (electromagnetic brakes or stirrers) are often used to control this flow.

The optimum flow pattern observed in the mould is a symmetric double roll flow as opposed to the single roll. The double roll flow allows for the impurities to rise to the free surface and as a result decreasing slug entrainment in the solid steel [15]. Implementing flow pattern control in the mould has proven to be a challenge due to the unavailability of suitable sensors to provide information about the flow inside the mould. Contactless Inductive Flow Tomography (CIFT) provides a solution for the above issue, as it allows us to reconstruct the velocity fields inside the mould, and thus giving us an idea of the flow patterns inside.

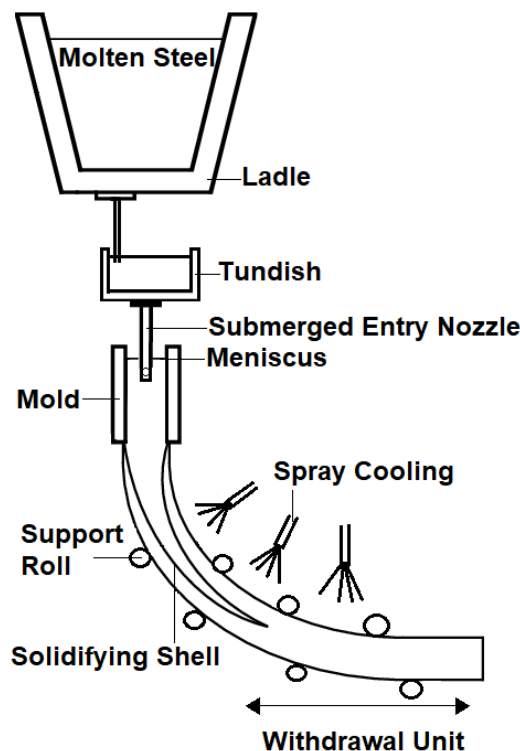


**Fig. 15:** Schematic of the Continuous Casting process



TOMOCON			GRANT AGREEMENT No.: 764902		
Deliverable Title: <b>Lab-type Integrated Controller Structures for TOMOCON Demonstrations</b>					
Del. Rel. No.	EU Del. No.	WP No.	Lead Beneficiary	Type	Date
D4.3.	D14	WP4	ULIB	Report	15.06.2021

### 3.2. Control loop

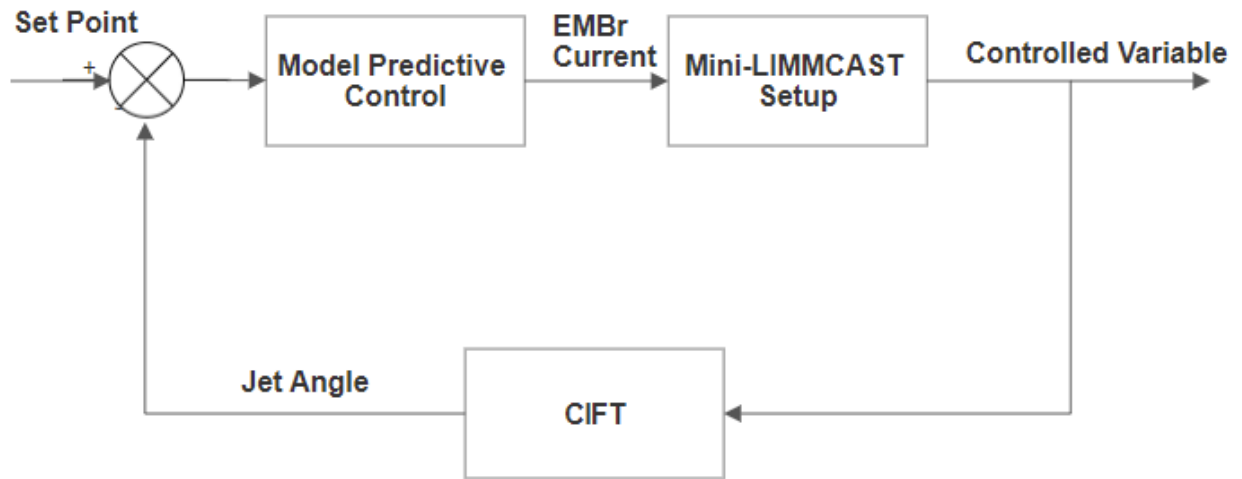


**Fig. 16:** Mini-LIMMCAST Control loop

The objective of the controller structure implemented on the Mini-LIMMCAST setup is to control the angle of the exiting jet from the SEN in order to avoid a deeper impingement into the mould. As seen in Fig. 16, CIFT will be used to obtain the controlled variable by extracting the jet angle from the reconstructed velocities. The controller based on MPC will use the current going to the Electromagnetic Brake (EMBr) to manipulate this angle of the jet.

### 3.3. Mini-LIMMCAST setup

The setup consists of a small-scale model of the mold and strand of a continuous slab caster. Gallium-indium-tin (GalInSn) eutectic alloy is used in place of the liquid steel because it is a liquid at room temperature. GalInSn is poured from the 'tundish' into an acrylic glass mold via the SEN as shown in Fig. 17. The flow rate in the SEN is controlled by a stopper rod. In order to run the experiments continuously, the melt flows from the bottom of the mold into the storage vessel, from which liquid is pumped back to the tundish to repeat the process. An electromagnetic brake is used to alter the flow in the mold. The Model Predictive Controller (MPC) is implemented using MATLAB/Simulink installed on the desktop connected to the Mini-LIMMCAST Setup (see Fig. 18). Communication between the controller and both the CIFT and Electromagnetic Brakes is done using TCP/IP protocol. In the end, the controller will receive the reconstructed velocity profile every sampling period and will send the required current value to the EMBr in order to achieve the desired jet angle set-point.





TOMOCON				GRANT AGREEMENT No.: 764902	
Deliverable Title: Lab-type Integrated Controller Structures for TOMOCON Demonstrations					
Del. Rel. No.	EU Del. No.	WP No.	Lead Beneficiary	Type	Date
D4.3.	D14	WP4	ULIB	Report	15.06.2021

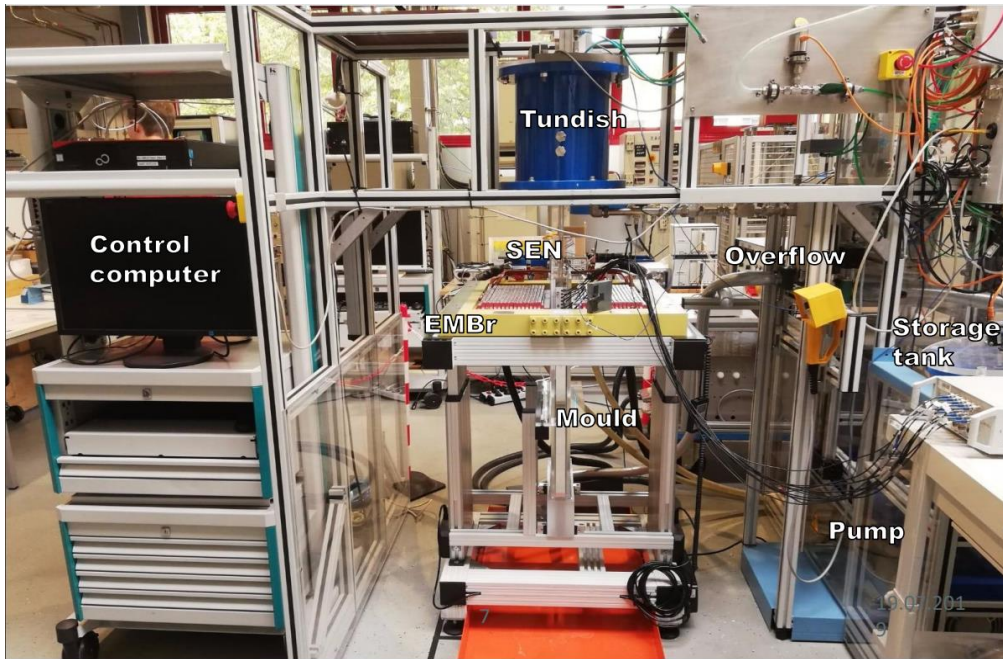


Fig. 17: Mini-LIMMCAST setup at HZDR

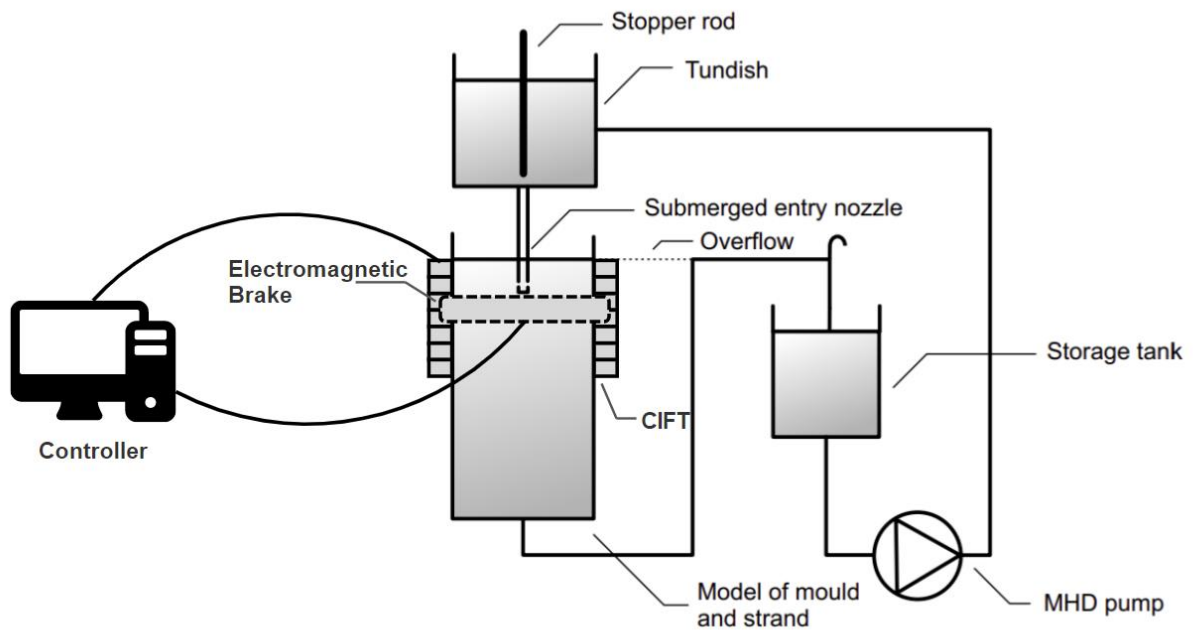


Fig. 18: Schematic of Mini-LIMMCAST with controller setup



TOMOCON			GRANT AGREEMENT No.: 764902		
Deliverable Title: <b>Lab-type Integrated Controller Structures for TOMOCON Demonstrations</b>					
Del. Rel. No.	EU Del. No.	WP No.	Lead Beneficiary	Type	Date
D4.3.	D14	WP4	ULIB	Report	15.06.2021

### 3.4. Electromagnetic brake

The main actuator in the proposed control loop is the electromagnetic brake. Electromagnetic actuation is commonly used to stabilize the turbulent flow in the mould. In the setup a static electromagnetic field is applied by the EMBr with the objective to control the angle of the exiting jet. The static electromagnetic field produced by the EMBr induces current in the conducting liquid, which generates a force that opposes the flow [16]. A wide “single ruler” EMBr is used to apply the magnetic field. The ruler is placed right below the outlet of the SEN instead of directly at the outlet level. It has been shown that this position for the brakes is better for stabilizing the jet flow [17]. The EMBr is controlled by varying the current going to the coils which results in variations to the magnetic field applied on the conductive liquid in the mould. Based on the decisions taken by the controller, the value for the current will be sent to the EMBr at each sample time.

### 3.5. Contactless Inductive Flow Tomography

Contactless Inductive Flow Tomography (CIFT) has been successfully implemented on the Mini-LIMMCAST setup and is used to reconstruct the velocity fields. The main concept of the CIFT technique relies on the flow of the conductive liquid going through a magnetic field created by the CIFT transmitter sensors. This creates electrical currents in the mould which results in an induced magnetic field. The induced magnetic field is measured by the receiver sensors and is used to reconstruct the velocity field in the mould (see Fig. 19) by solving the linear inverse problem.

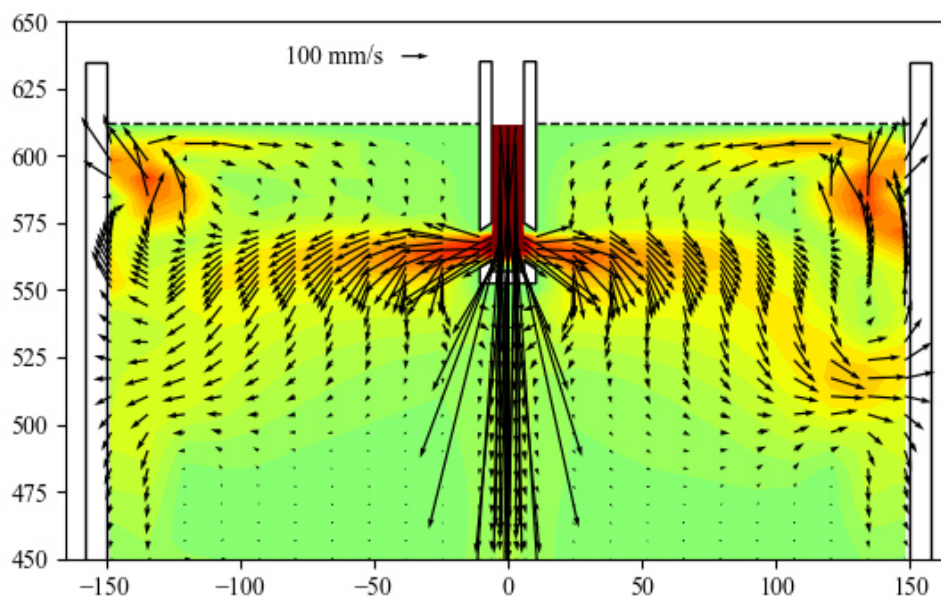


**Fig. 19:** Reconstructed velocity fields from CIFT



TOMOCON				GRANT AGREEMENT No.: 764902	
Deliverable Title: Lab-type Integrated Controller Structures for TOMOCON Demonstrations					
Del. Rel. No.	EU Del. No.	WP No.	Lead Beneficiary	Type	Date
D4.3.	D14	WP4	ULIB	Report	15.06.2021

## 3.6. Controller structure

### 3.6.1. Pre-processing of data

The pre-processing of the data is done by the Matlab Function “CalculateAngle” as seen in Fig. 20. The function calculates the angle per sampling time using the measured velocities from the CIFT. The function concentrates on the left half of the region of the mould. The direction of the velocity measured is identified by the sign of the velocity; negative velocities indicate that the flow is moving towards the sensors and mould wall, while positive velocities indicate that the flow is moving away from the sensors and mould wall. In order to track the movement of the jet, we need to compute the largest velocities with negative sign measured in the region surrounding the SEN outlet.

During every frame captured by the sensors, the algorithm compares the velocities and computes the y-axis position of the most negative velocities. This is done for the majority of the points between the mould wall and the SEN; however, the algorithm avoids taking the velocities near the mould wall. The velocities too near to the mould wall are strongly fluctuating due to the high turbulence occurring from the jet hitting the wall of the mould. Therefore, these strongly fluctuating velocities are not considered when calculating the jet angle. After the most negative velocities have been computed, linear regression using least squares is used to fit a line that would represent the flow of the jet. The linear regression uses the quadratic loss function to calculate the error in the model.

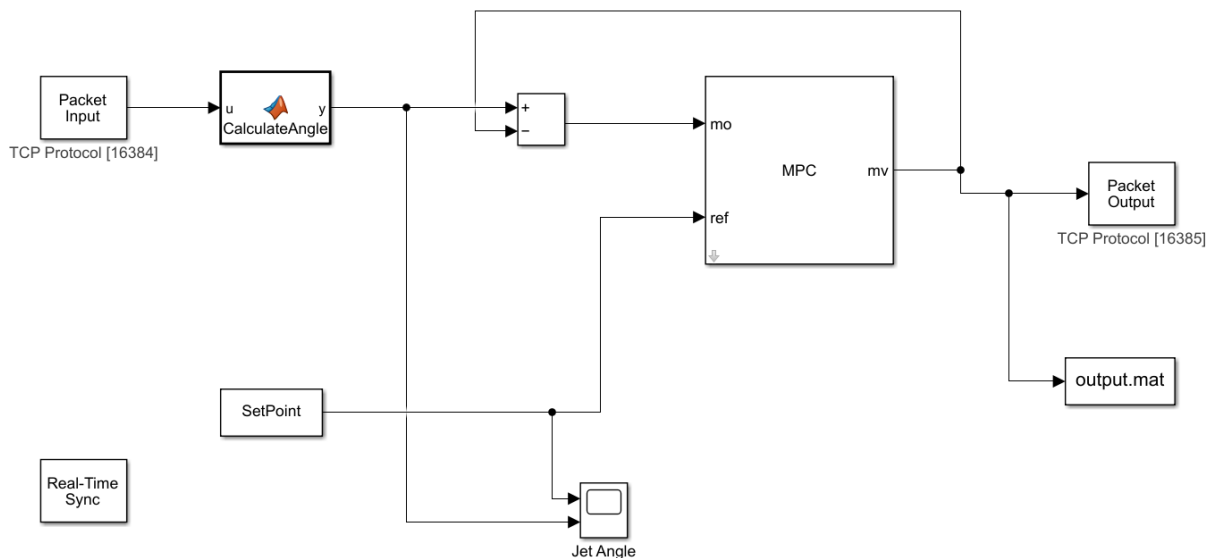


**Fig. 20:** Control loop implementation using Simulink

### 3.6.2. Testing

Before implementing the controller on the Mini-LIMMCAST setup, the MPC needs to be tested on a physical model. This is done through Hardware-in-the-loop simulation where



TOMOCON				GRANT AGREEMENT No.: 764902	
Deliverable Title: <b>Lab-type Integrated Controller Structures for TOMOCON Demonstrations</b>					
Del. Rel. No.	EU Del. No.	WP No.	Lead Beneficiary	Type	Date
D4.3.	D14	WP4	ULIB	Report	15.06.2021

the model is designed through system identification. By using previous experimental data from the setup, a linear model is used to describe the relationship between the EMBr current, and the jet angle similarly done in [18] using UDV data. By varying the current to the EMBr and recording the velocity fields measured by the CIFT, we are able to extract the angle of the jet from the velocity fields. Fig. 21 shows similar experiments done using UDV sensors; the figure shows that a first order model is sufficient to describe the relationship between the manipulated variable and the controlled variable. Based on this process model, the MPC is designed and tested using Hardware-in-the-loop simulation to see how the controller responds in real time to realistic virtual stimuli. Therefore, instead of using the experimental setup, a real-time computer is used as a virtual representation of the setup. The controller performance is evaluated and adjusted according to the simulation results.

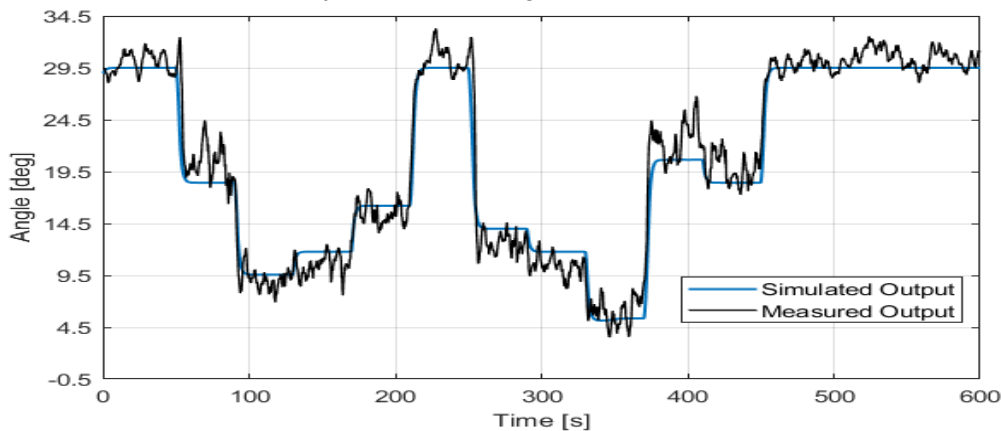


**Fig. 21:** Comparison of simulated model output with measured output using UDV

### 3.6.3. Implementation

As shown in Fig. 20, a Simulink model is used to execute the controller in real time. The model is applied on a Desktop Computer using Simulink Desktop Real-Time kernel; the computer has an Intel processor i5-7400 with 16 GB RAM. The model receives the reconstructed velocities from CIFT through TCP/IP. The reconstructed velocities will be used to calculate the angle of the jet. The controller will compare this angle with the set-point value and take a decision on how to manipulate the current to the brakes in order to track the changes to the set-point. The current value will be sent to the EMBr through TCP/IP. The Real-Time Sync block will be used to have the model run in real time. The controller itself is based on MPC; the main theory behind this control technique is the iterative, finite-horizon optimization of an internal plant model using a cost function  $J$  over the receding horizon. In this case, the cost function consists of the sum of three terms:

$$J(z_k) = J_y(z_k) + J_{\Delta u}(z_k) + J_e(z_k) \quad (4)$$

where  $z_k$  is the vector of the quadratic program decision variables.  $J_y(z_k)$  refers to the output reference tracking,  $J_{\Delta u}(z_k)$  is for the manipulated variable move suppression, and  $J_e(z_k)$  refers to constraint violations as seen below:



TOMOCON				GRANT AGREEMENT No.: 764902	
Deliverable Title: Lab-type Integrated Controller Structures for TOMOCON Demonstrations					
Del. Rel. No.	EU Del. No.	WP No.	Lead Beneficiary	Type	Date
D4.3.	D14	WP4	ULIB	Report	15.06.2021

$$J_y(z_k) = \sum_{j=1}^{n_y} \sum_{i=1}^p \left\{ \frac{w^y_{i,j}}{s^y_j} [r_j(k+j|k) - y_j(k+j|k)] \right\}^2 \quad (5)$$

$$J_{\Delta u}(z_k) = \sum_{j=1}^{n_u} \sum_{i=0}^{p-1} \left\{ \frac{w^{\Delta u}_{i,j}}{s^u_j} [u_j(k+i|k) - u_j(k+j-1|k)] \right\}^2 \quad (6)$$

$$J_e(z_k) = \rho_\varepsilon \varepsilon_k^2 \quad (7)$$

where  $k$  is the current control interval,  $p$  is the prediction horizon,  $n_y$  and  $n_u$  are the number of plant output variables and number of manipulated variables.  $y_j(k+j|k)$  and  $r_j(k+j|k)$  are the predicted value and reference value of  $j$ -th plant output at  $i$ -th prediction horizon.  $s^y_j$  and  $s^u_j$  are the scale factor for  $j$ -th plant output and manipulated variable, respectively.  $w^y_{i,j}$  and  $w^{\Delta u}_{i,j}$  are the tuning weights for the  $j$ -th plant output and manipulated variable movement at  $i$ -th prediction horizon.  $\varepsilon_k$  is the slack variable at control interval  $k$ .  $\rho_k$  is the constraint violation penalty weight [19].

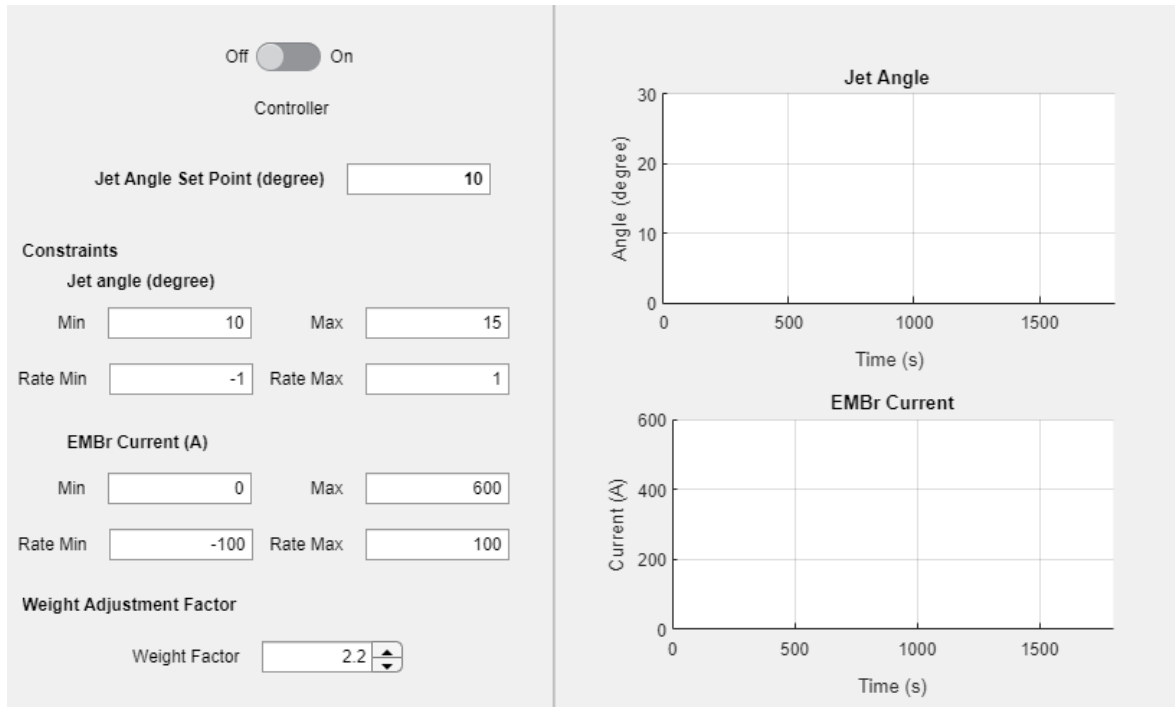


**Fig. 22:** Graphical User Interface used to tune the MPC for Jet Angle Control

A further step can be taken where a Graphical User Interface is created in order to simplify the control part of the setup. As seen in Fig. 22 the interface will allow the user to monitor the manipulated variable and the controlled variable. Additionally, the user can adjust the set-point for the jet angle and adjust the performance of the controller. This can be done through adjusting the constraints on both the manipulated variable and the controlled

<b>TOMOCON</b>			<b>GRANT AGREEMENT No.: 764902</b>		
Deliverable Title: <b>Lab-type Integrated Controller Structures for TOMOCON Demonstrations</b>					
<b>Del. Rel. No.</b>	<b>EU Del. No.</b>	<b>WP No.</b>	<b>Lead Beneficiary</b>	<b>Type</b>	<b>Date</b>
D4.3.	D14	WP4	ULIB	Report	15.06.2021

variable. Furthermore, the weight factor will allow the user to control how aggressive or robust the closed loop response will be.

Lastly, argon gas injection will be introduced as a disturbance to the controller in the Mini-LIMMCAST setup. Argon gas is typically used in the SEN to prevent slug entrapment [20]; however, the injection of the bubbles can cause undesirable flow behavior in the mould and significantly affect the jet angle. Argon gas will be periodically injected into the SEN; the controller will be required to reject the disturbance and keep the set-point within optimum values while not exceeding the constraints on the EMBr current.





TOMOCON			GRANT AGREEMENT No.: 764902		
Deliverable Title: <b>Lab-type Integrated Controller Structures for TOMOCON Demonstrations</b>					
Del. Rel. No.	EU Del. No.	WP No.	Lead Beneficiary	Type	Date
D4.3.	D14	WP4	ULIB	Report	15.06.2021

## 4. Demonstration Process: Inline Swirl Flow Separator

### 4.1. Introduction

This report describes the equipment and codes used in the demonstration of the Tomography-Controlled Inline Swirl Separator developed in the TOMOCON project. It starts with a detailed description of the hardware used in the control of the system, and later describes the design and implementation of the controller in the loop.

### 4.2. System hardware

A simplified schematics of the separator used in the demonstration is presented in Fig. 23. There are two control valves installed in the device: The pickup tube valve, used to control the separation process, and the outer outlet valve, used to set a local backpressure that bends the flow towards the pickup tube. As a simplification this valve is not used for real time control, but to set the operating point of the system.

Both control valves present a strong hysteretic behavior, which requires the control actions to be corrected to generate the desired output, accounting for the nonlinear term. To build such term, a deep analysis of the behaviour of the valve was performed. The complexity of the behaviour is the main reason behind the use of a single controller output in this proof-of-concept demonstration.

The separation process is monitored using Electrical Resistance Tomography (ERT) via a sensor provided by Rocsole with 16 electrodes. The sensor data is not reconstructed into an image to speed it up, being replaced by a personalized algorithm developed by ESRs 4 and 10. The algorithm converts current measurements by the device into the average gas core diameter, and will be described in detail in Deliverable 2.4. The sensor presents a temporal resolution up to 12 Hz and it is used at 10 Hz in this work.

The control actions are computed in LabVIEW by a desktop computer, that was already used to send the steering voltages and currents in the remaining loop sensors and valves. The computer is a Dell Optiplex 9020, with 8 GB of RAM memory and an Intel i5-4590 processor.



TOMOCON			GRANT AGREEMENT No.: 764902		
Deliverable Title: <b>Lab-type Integrated Controller Structures for TOMOCON Demonstrations</b>					
Del. Rel. No.	EU Del. No.	WP No.	Lead Beneficiary	Type	Date
D4.3.	D14	WP4	ULIB	Report	15.06.2021

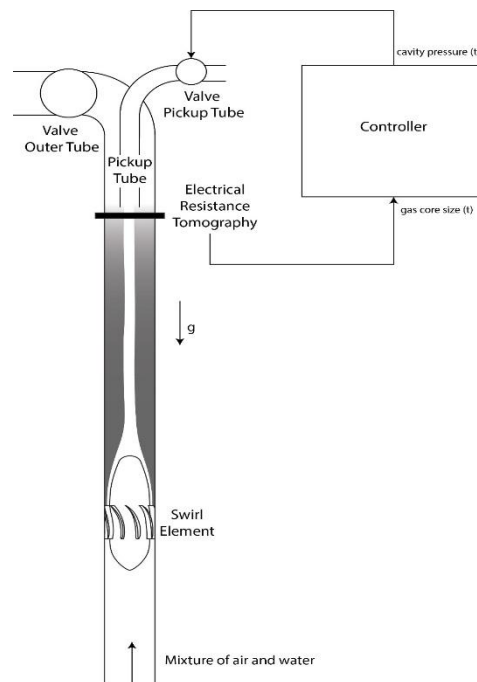


**Fig. 23:** Tomography-Controlled Inline Swirl Separator schematics

#### 4.2.1. Valve behavior and dynamics

The control valves presented in Fig. 23 are pneumatic Stübbe MV 310 diaphragm valves; the pickup tube valve is DN25, and the outer tube valve is DN50. Diaphragm valves present their openings imposed by the air pressure in their cavity, that balances a spring. Both valves are normally open, meaning that they are totally open when no pressure is imposed in their cavity.

##### 4.2.1.1. Pressure regulator response

SMC ITV 2050 pressure regulators are used in this work to control the valve opening. The devices present two internal linear solenoid valves, one to increase the cavity pressure by allowing the passage of air between the supply and the valve, and one to reduce the cavity pressure by releasing air to the lab, as presented in Fig. 24.

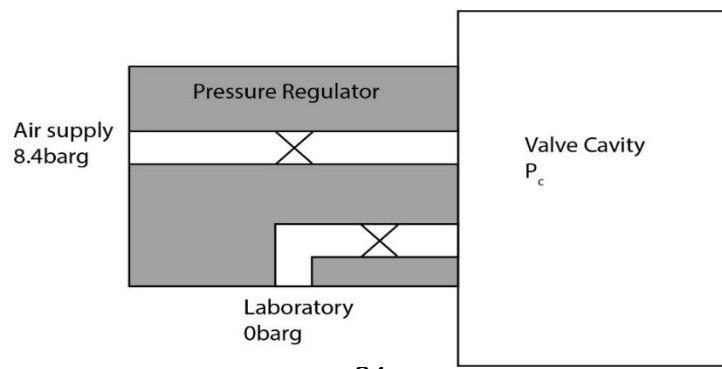


**Fig. 24:** Pressure regulator schematics

Dissemination Level: **Public**



This project has received funding from the European Union's Horizon 2020 research and innovation programme under the Marie Skłodowska-Curie Grant Agreement No. 764902.

TOMOCON				GRANT AGREEMENT No.: 764902	
Deliverable Title: <b>Lab-type Integrated Controller Structures for TOMOCON Demonstrations</b>					
Del. Rel. No.	EU Del. No.	WP No.	Lead Beneficiary	Type	Date
D4.3.	D14	WP4	ULIB	Report	15.06.2021

Since the flow rate crossing the ducts inside the pressure regulator is determined by the pressure drop along the path, and the valve typically requires a low pressure to operate (the pickup tube valve is fully closed below 1 barg and the outer tube valve is fully closed below 2 barg), the flow of air from the air supply at a high pressure to the valve cavity is much greater than the outflow of air from the cavity to the lab, that experiences a lower pressure drop, which causes the valve to close much faster than open. The behavior is illustrated in Fig. 25, where the average of 5 experiments considering the pressure regulator connected to the pickup tube valve is presented. The response is measured by a pressure gauge at the location at 10 Hz.

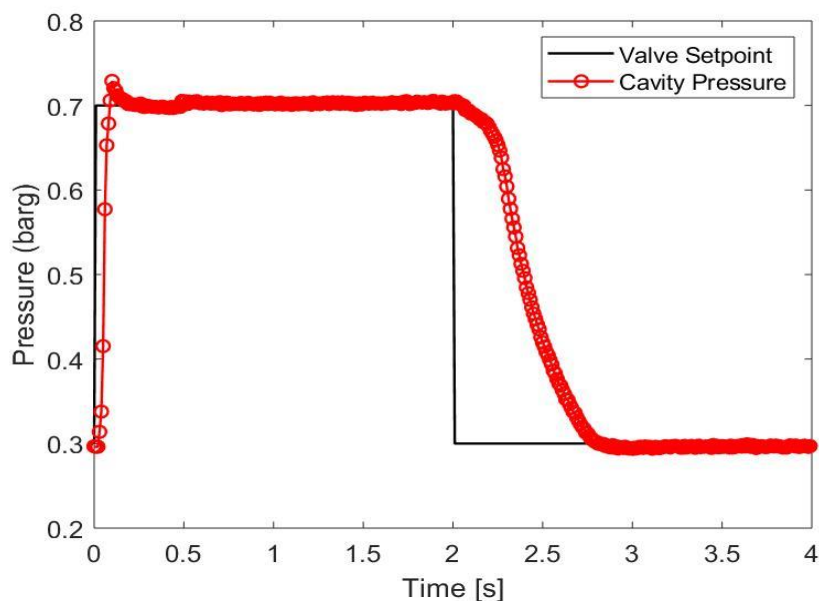


**Fig. 25:** Step response of the pressure regulator connected to the pickup tube valve

The 0.09 s required for the valve to go from 0.3 to 0.7 is acceptable, but the 0.8 s required for the return is too slow for the process, even if the valve dynamics are negligible. To speed up the opening response of the system, a second pressure regulator is installed connected to the other side of the membrane of the valve, acting as a counter pressure and allowing it to operate at higher input pressures. The pickup tube valve is operated in the range of 4 to 5 barg, where the desired pressure is achieved around 0.1 s in both directions after the change in the setpoint between 4.3 and 4.7 barg. A picture of the pickup tube valve with the 2 pressure regulators installed is presented in Fig. 26.



TOMOCON			GRANT AGREEMENT No.: 764902		
Deliverable Title: <b>Lab-type Integrated Controller Structures for TOMOCON Demonstrations</b>					
Del. Rel. No.	EU Del. No.	WP No.	Lead Beneficiary	Type	Date
D4.3.	D14	WP4	ULIB	Report	15.06.2021

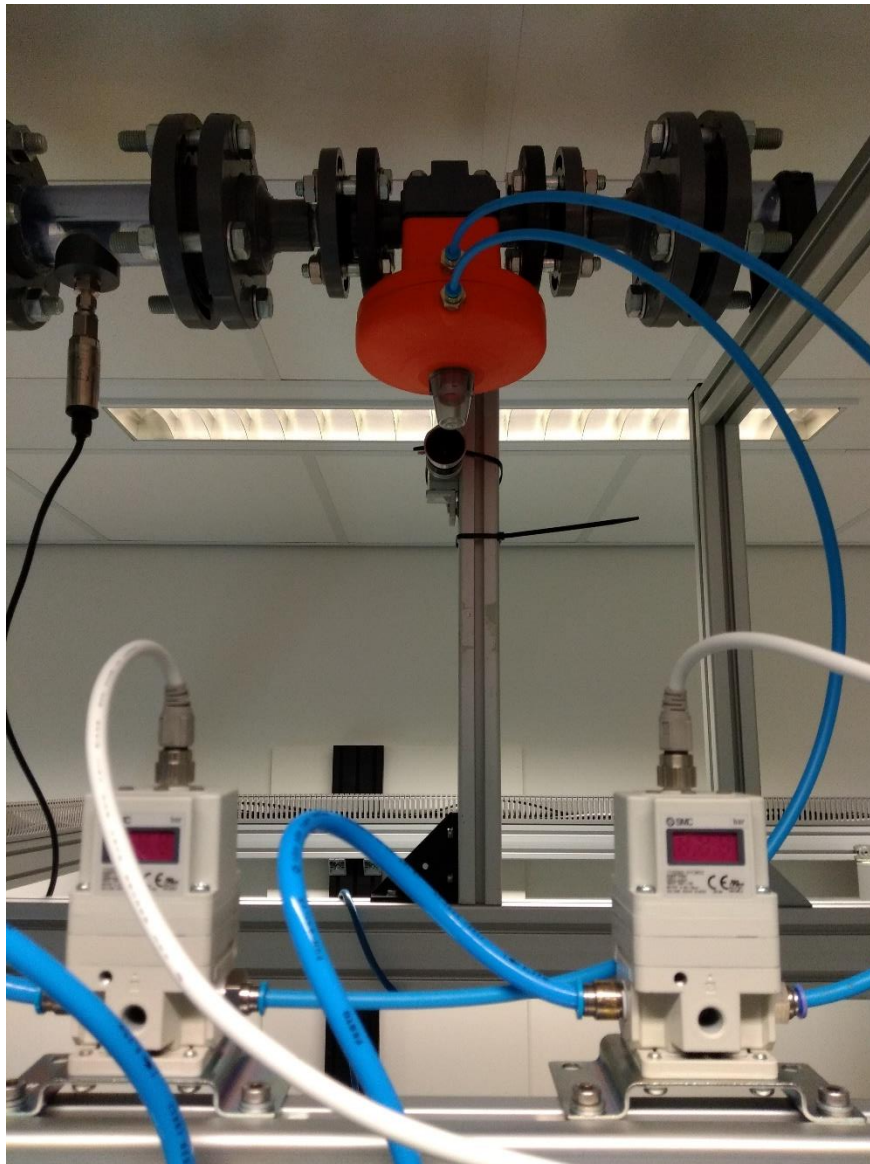


**Fig. 26:** Pickup tube control valve with pressure regulators

#### 4.2.1.2. Valve hysteresis

Changing the cavity pressure is just the first step towards the motion of the valve. The membrane of the valve is connected to a stem, and presents its own inertia and damping due to friction. Moreover, as the membrane is deformed when closing the valve, it presents its own resistance to the motion of the stem. It was observed that the valve presents a strong hysteretic behavior, such that its position is dependent on the history of the previous inputs. When slowly varying the cavity pressure and waiting for the stem to reach steady state, the valve generates the contour plots of position of Fig. 27.



TOMOCON				GRANT AGREEMENT No.: 764902	
Deliverable Title: <b>Lab-type Integrated Controller Structures for TOMOCON Demonstrations</b>					
Del. Rel. No.	EU Del. No.	WP No.	Lead Beneficiary	Type	Date
D4.3.	D14	WP4	ULIB	Report	15.06.2021

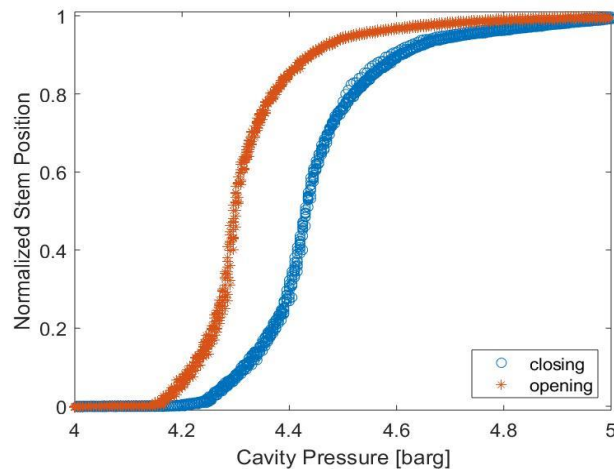


**Fig. 27:** Pickup tube valve hysteresis boundary

The behavior of intermediary inputs is complicated and not fully modelled in a first controller. Instead, the average curve and the distance between the average and the closing curve are fitted according to:

$$\bar{p}_c(x) = 0.3872 x^4 + 0.5378 x^3 - 1.2647 x^2 + 0.7692 x + 0.2057 \quad (8)$$

$$\delta p(x) = 0.1153 x^4 - 0.0460 x^3 - 0.1302 x^2 + 0.1221 x + 0.0363 \quad (9)$$

Where the closing curve is described by  $\bar{p}_c + \delta p$  and the opening curve by  $\bar{p}_c - \delta p$ .

#### 4.2.1.3. Flow coefficient

Although the position of the stem presents a strong hysteretic behavior, the same does not occur for the flow coefficient imposed by the valve. The flow coefficient, that determines how the flow behaves in the region, is a piecewise linear function of the stem position, as presented in Fig. 28. As a consequence, the entire action of the valve can be described based on the stem position.

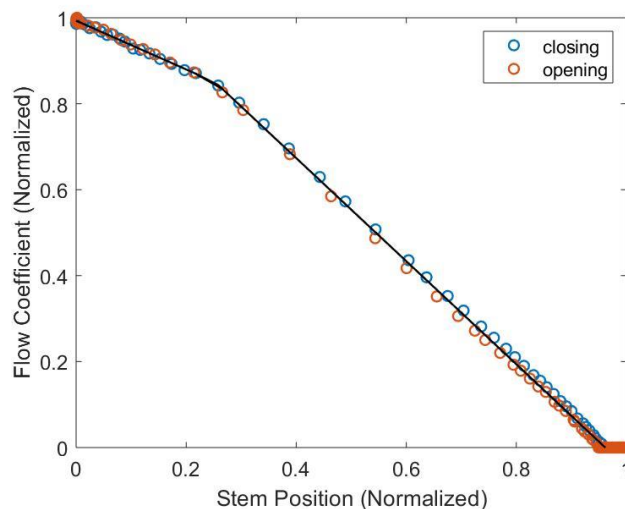


**Fig. 28:** Flow coefficient as a function of the stem position



TOMOCON				GRANT AGREEMENT No.: 764902	
Deliverable Title: Lab-type Integrated Controller Structures for TOMOCON Demonstrations					
Del. Rel. No.	EU Del. No.	WP No.	Lead Beneficiary	Type	Date
D4.3.	D14	WP4	ULIB	Report	15.06.2021

#### 4.2.1.4. Stem dynamics

The valve membrane and stem are modelled according to:

$$m\ddot{x} + c\dot{x} + f(x) = p_c(t) A + f_0, \quad (10)$$

where  $x$  is the stem position,  $A$  is the projected area of the membrane,  $f(x)$  is the hysteresis and spring forces and  $f_0$  is the normal force of the wall of the valve balancing the spring (linear term of  $f(x)$ ) when  $x = 0$ .

It is hard to precisely recover the mass,  $m$ , and damper,  $c$ , terms via system identification techniques without studying in detail the behavior of the hysteretic force for smaller cycles, because of the history component of the non-linear spring force,  $f(x)$ , that can be very different from equations (8) and (9). However, it was observed that the behavior of the hysteretic force is symmetric when loading/unloading the device via periodic inputs, which allows to track the Gain and Phase of the stem for different frequencies of excitation. The approach leads to the Bode plot of Fig. 29, that is well approximated considering:

$$\begin{aligned} m &= 0.0424 \\ c &= 0.28 \\ k &= 0.6934 \\ A &= 1.4155 \end{aligned} \quad (11)$$

The coefficients show that the inertia of the stem is relatively small when compared to the damper and spring terms.

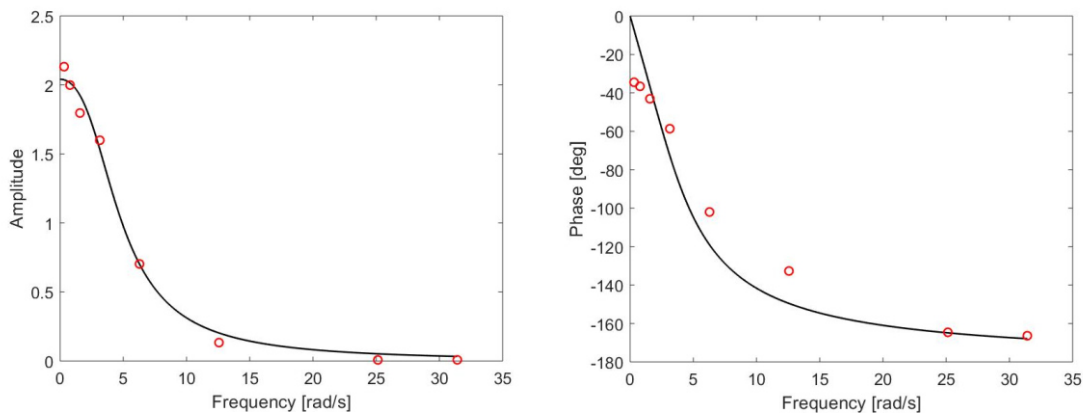


Fig. 29: Bode plot of the valve

### 4.3. Control loop and software implementation

#### 4.3.1. Operating point and disturbances

The flow rates of air and water are imposed in the loop using a pump and a mass flow controller. The pump frequency is maintained fixed during the control, and disturbances are applied in the gas flow rate by changing the setpoint of the mass flow controller. Since the





TOMOCON				GRANT AGREEMENT No.: 764902	
Deliverable Title: Lab-type Integrated Controller Structures for TOMOCON Demonstrations					
Del. Rel. No.	EU Del. No.	WP No.	Lead Beneficiary	Type	Date
D4.3.	D14	WP4	ULIB	Report	15.06.2021

pump provides a fixed power to the flow, and the pressure distribution in the system changes when changing the percentage of air or acting on the valves, the water flow rate continuously oscillates during the experiments.

The system is designed to operate at  $V_{sl} = 0.4\text{m/s}$  and  $V_{sg} = 0.25\text{m/s}$ , conditions where churn flow is present upstream the swirl separator. The condition is chosen since it leads to a gas core more-or-less at the same size of the pickup tube, allowing for an effective control of the separation and evaluation of the gains of the approach. Moreover, the relatively large core is required for the measurements performed by the ERT system, that has a poor sensibility in the center of the pipe and cannot see small cores.

The core continuously oscillates at the frequency of the passage of the Taylor bubbles due to the churn flow upstream the separator. Because the time scales caused by the churn fluctuations are smaller than the time scales of the system when acting on the valve, these high oscillations of the churn flow act as a high-amplitude noise, and must be filtered out from the low frequency behavior of the system. Fig. 30 shows the response of the system for a square wave at 0.1 Hz in the valve position, where the fitted transfer function presents the average behavior of the core, without the churn fluctuations.

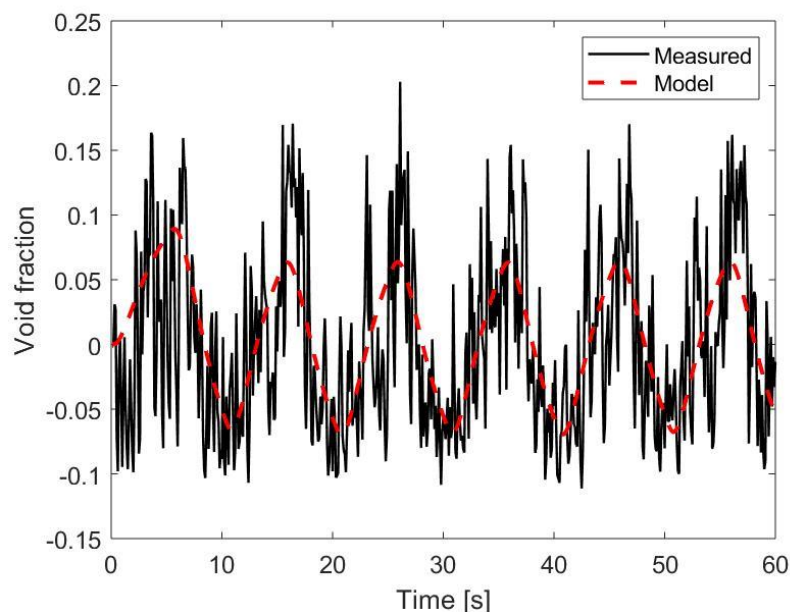


**Fig. 30:** Void fraction measured (continuous line) and modelled (dashed line). The high frequency oscillations are connected to the churn flow upstream, and cannot be controlled. Response to a square wave at 0.1 Hz around the operating point of the system.

The core dynamics when acting on the pickup tube valve is described by:





TOMOCON			GRANT AGREEMENT No.: 764902		
Deliverable Title: Lab-type Integrated Controller Structures for TOMOCON Demonstrations					
Del. Rel. No.	EU Del. No.	WP No.	Lead Beneficiary	Type	Date
D4.3.	D14	WP4	ULIB	Report	15.06.2021

$$\frac{\alpha(s)}{X(s)} = \frac{0.1376}{s^2 + 1.537s + 0.3647} \quad (12)$$

Which leads to a controllable and observable system when converted to a state space representation.

### 4.3.2. The controller

A PI controller is designed for the process, with the integral term designed to compensate the non-linearities of the valve. Due to the large fluctuations of the churn flow, the performance of the system is poor if controlled without a filter of the output. To overcome the instability brought to the performance of the separator when acting directly on the sensor output, an observer is designed to predict the states of the process, in special the mean void fraction of the system, and the estimated states are used for the feedback action.

The strong hysteresis of the valve affects the movement of stem such that a totally different valve output (stem position) is obtained for the same input. Therefore, proportional actions designed to between the valve cavity pressure and the ERT measurement are highly ineffective, and the system would be controlled mainly by the integral action. To keep the proportional term effective, a model of the valve must be used to adjust the input to achieve an optimal performance of the system.

Since the response of the system is directly connected to the stem position, the control loop is designed between the stem position and the core size, and an inverse model of the valve is used to predict the cavity pressure required for the desired position. The obtained control loop is illustrated in Fig. 31.

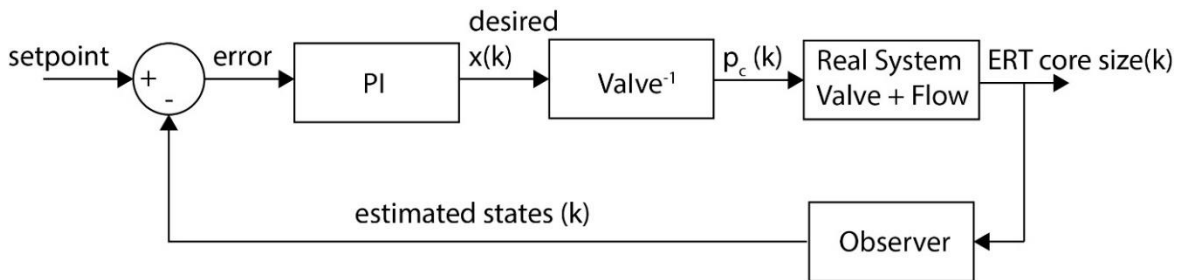


**Fig. 31:** Control loop used in the experiments

An anti-windup term is added to the PI controller such that the integral term is limited when  $x$  is saturated.

#### 4.3.2.1. Details on the inverse valve term

The inverse model of the valve corresponds has several components. It is designed considering the average non-linear spring force, given by equation (8) ( $f(x) \approx A\bar{p}_c(x) + f_0$ ). Then, to get the desired output  $x(k)$ , a cavity pressure should be according to:



TOMOCON			GRANT AGREEMENT No.: 764902		
Deliverable Title: <b>Lab-type Integrated Controller Structures for TOMOCON Demonstrations</b>					
Del. Rel. No.	EU Del. No.	WP No.	Lead Beneficiary	Type	Date
D4.3.	D14	WP4	ULIB	Report	15.06.2021

$$p_c(k) = \frac{1}{A} \left\{ \left[ \frac{m}{\Delta t^2} + \frac{c}{\Delta t} \right] x(k) - \left[ \frac{2m}{\Delta t^2} + \frac{c}{\Delta t} \right] x(k-1) + \frac{m}{\Delta t^2} x(k-2) + A\overline{p}_c(x) \right\} \quad (13)$$

The calculated pressure requires a correction depending on the direction of the input, which is implemented as a bang-bang action of amplitude  $\delta p$  (equation (9)). This bang-bang term has a gain of 1 when the desired  $x$  is bigger than the previous value (closing action), and -1 when the desired  $x$  is smaller than the previous value, to compensate for the different force required to get the same stem position depending on the direction of the input. In addition to that, the term is damped when the error is small, such that no strong changes valves are made when the system is around the optimal point of operation.

### 4.3.3. Controller and observer gains and implementation

The results of the final demonstration are currently under obtainment. Although the approach is highly promising, and the structure is ready and was partially tested, some fine tuning of the controller and observer gains is still required, and the values will be reported together with the results of the approach. The designed controller is implemented in LabVIEW as a discrete time actuator with a frequency of 10 Hz.



TOMOCON				GRANT AGREEMENT No.: 764902	
Deliverable Title: <b>Lab-type Integrated Controller Structures for TOMOCON Demonstrations</b>					
Del. Rel. No.	EU Del. No.	WP No.	Lead Beneficiary	Type	Date
D4.3.	D14	WP4	ULIB	Report	15.06.2021

## 5. Demonstration Process: Microwave Drying

### 5.1. Introduction

The microwave drying process is becoming an attractive candidate for drying high moisture materials in many industrial applications such as food preservation, wood processing, and heat insulation industries. Volumetric and selective heating features in microwave drying result in the fast internal evaporation of moisture. In this process, the wet material, which is a quasi-continuous wet polymer foam with 3 x 50 cm in cross-section, is exposed to several microwave sources in an oven cavity until the water inside the material evaporates. One of the main goals is to reach a certain level of moisture distribution inside the material after the drying process. Our research aims to design and integrate tomographic sensors with an advanced moisture controller to achieve this goal.

### 5.2. Sensors and control structure

Two tomographic sensors are assisting the controller. An electrical capacitance tomography (ECT) sensor is installed at the end of the process, estimating the foam permittivity percentage after the drying process as the system output correlated with the material moisture. The input foam entering the oven cavity does not have constant moisture. The variation in the input foam moisture is considered as a disturbance to the process measured by the microwave tomography (MWT) sensor.

A feedback controller with different techniques such as PI, LQG, and MPC is designed to track the set point moisture for the foam. This controller receives the moisture information of the foam from the ECT, compares it with the setpoint, and calculates the power level of the microwave sources needed to track the set point. With the PI control structure, a feedforward control loop is also added to reject the disturbance applying to the system. The feedforward controller receives the information from the MWT and adds a control signal to the feedback controller command. Fig. 32 shows the structure of the feedback-feedforward controller with the sensor connection.

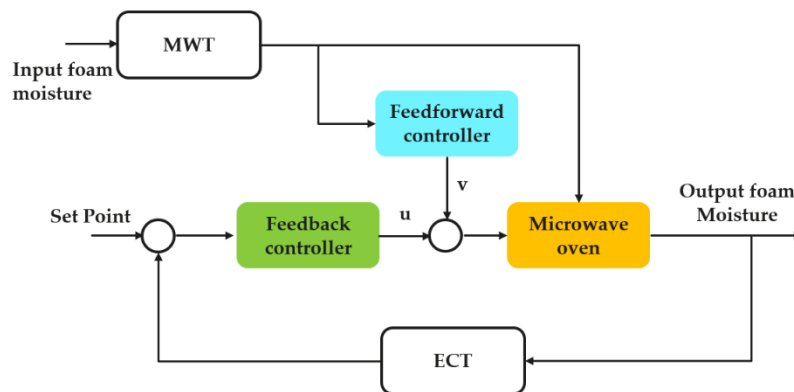


**Fig. 32:** A schematic of the controller structure and the tomographic sensors connections



TOMOCON				GRANT AGREEMENT No.: 764902	
Deliverable Title: <b>Lab-type Integrated Controller Structures for TOMOCON Demonstrations</b>					
Del. Rel. No.	EU Del. No.	WP No.	Lead Beneficiary	Type	Date
D4.3.	D14	WP4	ULIB	Report	15.06.2021

## 5.3. The microwave system and hardware connections

### 5.3.1. Microwave system

Our testbed system is called HEPHAISTOS, a large-scale microwave oven located at Karlsruhe Institute of Technology (KIT), Germany. The oven includes three cavity modules, each 100 cm in length. Since the system is an open oven, two microwave filters, each 150 cm in length, are installed at both sides of the oven to block the microwave power leakage from the entering and exit points. The whole length of the system is 729 cm.

A picture of this device is shown in Fig. 33. The system is operated by software named SIMPAC developed by the manufacturing company of the microwave system, Vötsch Industrietechnik GmbH, Germany, which is also an associated partner in TOMOCON. The microwave sources installed are 18 magnetrons operating at 2.45 GHz with 2 kW power each, which results in the evaporation of the foam moisture. Moreover, there is hot air circulating in the device to remove the evaporated moisture. Through the SIMPAC, the power levels of all the microwave sources, which are the actuators of this process, can be controlled. However, it is not possible to adjust the power levels individually with this software. The hot air temperature and the conveyor belt speed are among other parameters which can be controlled using SIMPAC. Fig. 34 shows the connection between the oven and SIMPAC on a computer desktop.

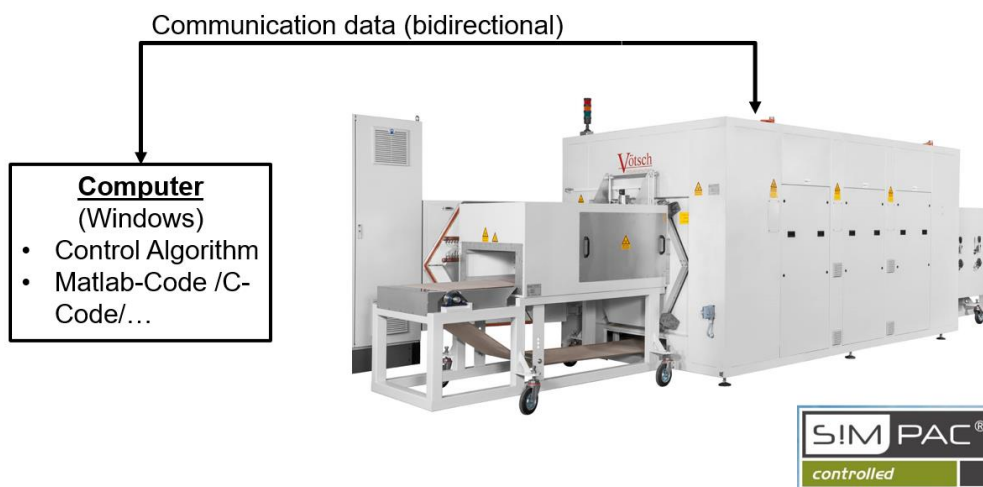


**Fig. 33:** A picture of the HEPHAISTOS microwave system located at KIT, Germany, with the communication objective

### 5.3.2. Control implementation

In our project, MATLAB software is used to design and test the control methods. Therefore, it is easier if, in the final demo, we can directly implement the controllers in MATLAB. The KIT team had already developed an interface to communicate with SIMPAC for their older project. However, it needed further modification, which involved hardware improvement in the microwave oven too. With the collaboration of KIT and Vötsch, it is now

<b>TOMOCON</b>			<b>GRANT AGREEMENT No.: 764902</b>		
Deliverable Title: <b>Lab-type Integrated Controller Structures for TOMOCON Demonstrations</b>					
<b>Del. Rel. No.</b>	<b>EU Del. No.</b>	<b>WP No.</b>	<b>Lead Beneficiary</b>	<b>Type</b>	<b>Date</b>
D4.3.	D14	WP4	ULIB	Report	15.06.2021

possible to implement the controller on a MATLAB m-file. The interface developed by KIT calls the m-file at a specific sample time, which can be modified too, and receives the data corresponding to the power level. Other parameters like the belt speed and hot air temperature are also sent to the interface, which are assumed to be constant during the process. Fig. 35 shows the connection of MATLAB, interface, and SIMPAC.

As shown in Fig. 36, a computer desktop is connected to the oven and the interface. The MATLAB software is installed on this computer to control and monitor the microwave oven. The connection between MATLAB and the interface is only to set the power levels, and the outputs of the sensors should be transferred through other means than the interface.

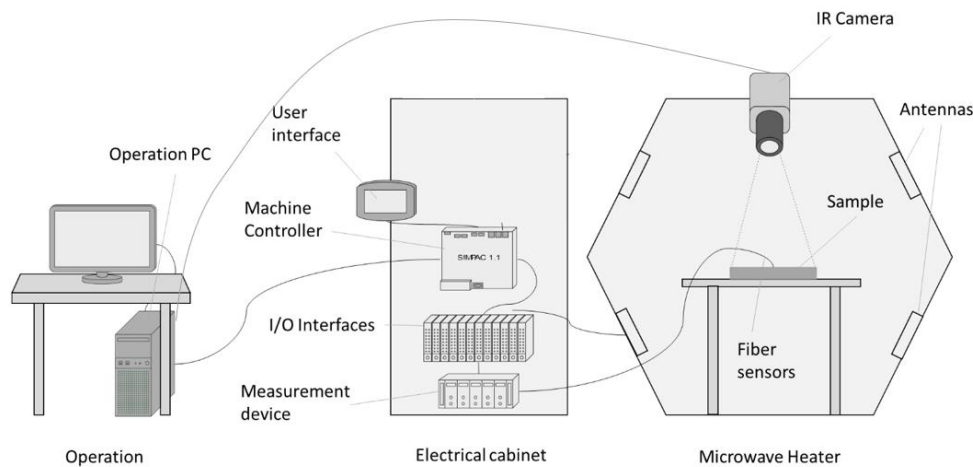


**Fig. 34:** The connection between SIMPAC and the microwave oven

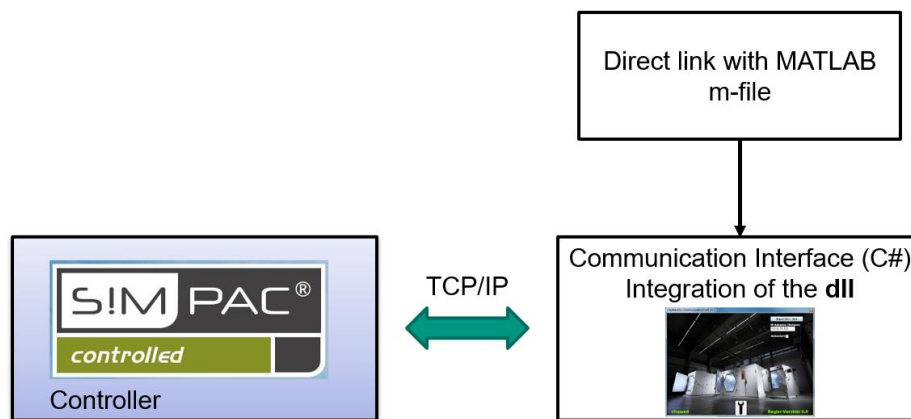


**Fig. 35:** MATLAB connection with the interface and the SIMPAC



TOMOCON			GRANT AGREEMENT No.: 764902		
Deliverable Title: <b>Lab-type Integrated Controller Structures for TOMOCON Demonstrations</b>					
Del. Rel. No.	EU Del. No.	WP No.	Lead Beneficiary	Type	Date
D4.3.	D14	WP4	ULIB	Report	15.06.2021



**Fig. 36:** The PC connecting the controller with the oven and the sensors

### 5.3.3. Sensor connections

The controller is implemented in MATLAB, and it needed to read the data from the ECT and MWT sensors directly to calculate the appropriate power level to track the set point.

The MWT sensor designed and developed by ESR 7 and ESR 15 is installed at the inlet of the HEPHAISTOS oven and estimates the moisture distribution in the polymer foam. The total time for the measurement and reconstruction is 0.8 s. The MWT sensor is connected to the computer running the controller via an Ethernet cable. The entire process of transferring data is automated using MATLAB. Fig. 37 shows a picture of this sensor while measuring the input foam moisture.

The ECT sensor developed by ESR 14 is installed at the outlet of the oven and estimates the moisture distribution in the polymer foam after the drying process, as shown in Fig. 38. The sensor is connected to a measurement device built by Rocsole Ltd., Kuopio, Finland. The measurement device applied AC voltage with the magnitude of 2.5 V and frequency of 625 kHz to the exciting electrodes and measured the inter-electrode capacitances. The measurements are transferred using an Ethernet cable in real-time to the MATLAB software installed on the computer connected to the oven. The measurement and the reconstruction takes less than a second.



**Fig. 37:** The MWT sensor installed at the inlet of the HEPHAISTOS oven





TOMOCON			GRANT AGREEMENT No.: 764902		
Deliverable Title: <b>Lab-type Integrated Controller Structures for TOMOCON Demonstrations</b>					
Del. Rel. No.	EU Del. No.	WP No.	Lead Beneficiary	Type	Date
D4.3.	D14	WP4	ULIB	Report	15.06.2021



**Fig. 38:** The ECT sensor installed at the outlet of the HEPHAISTOS oven

## 5.4. System identification and control methods

The dynamic model of the oven was obtained using system identification tools. For the input-output data used in the system identification process, the power level of all microwave sources was taken as the system input, and the ECT output, which is the permittivity percentage on the wet basis, was taken as the system output. The permittivity percentage on a wet basis is correlated with the moisture percentage of the foam. A state-space model of the system is calculated, which allows several control methods. So far, the PI control, fuzzy PI, linear quadratic gaussian (LQG) control, and model predictive control (MPC) have been designed for this process, and some have already been experimented. Fig. 39 shows the system output measured by the ECT sensor when a PI controller was implemented on the system. As can be seen, the system output nicely followed the setpoint despite the input disturbance. Here, the feedforward loop is not connected yet. The command control, which is the power level of the microwave sources in percentage, is also illustrated in Fig. 40.

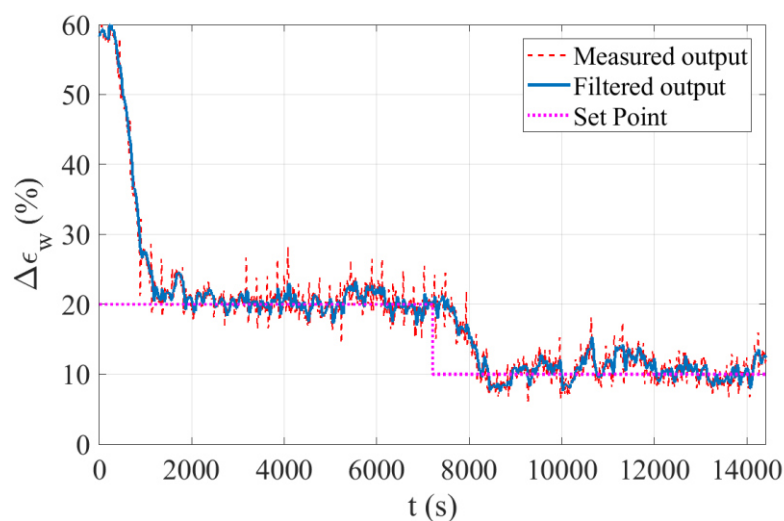


**Fig. 39:** The output foam permittivity measured by the ECT sensor while a PI controller is implemented



TOMOCON			GRANT AGREEMENT No.: 764902		
Deliverable Title: <b>Lab-type Integrated Controller Structures for TOMOCON Demonstrations</b>					
Del. Rel. No.	EU Del. No.	WP No.	Lead Beneficiary	Type	Date
D4.3.	D14	WP4	ULIB	Report	15.06.2021

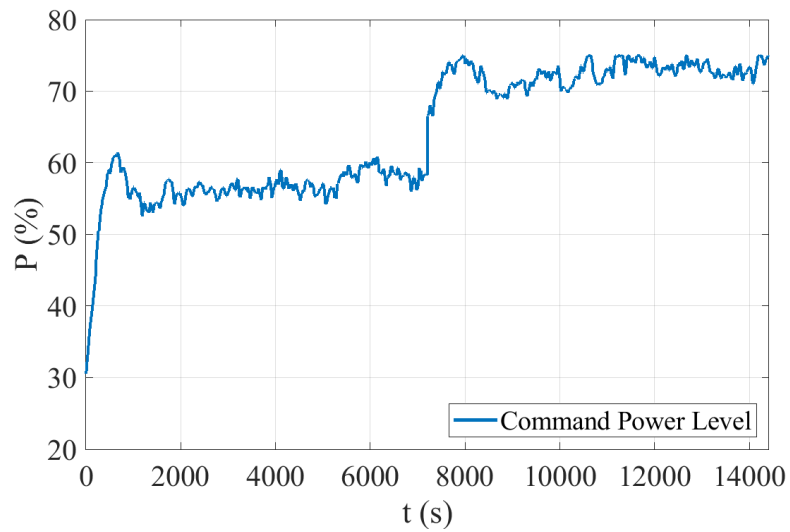


**Fig. 40:** The control command of a PI controller to the microwave sources



<b>TOMOCON</b>				<b>GRANT AGREEMENT No.: 764902</b>	
Deliverable Title: <b>Lab-type Integrated Controller Structures for TOMOCON Demonstrations</b>					
<b>Del. Rel. No.</b>	<b>EU Del. No.</b>	<b>WP No.</b>	<b>Lead Beneficiary</b>	<b>Type</b>	<b>Date</b>
D4.3.	D14	WP4	ULIB	Report	15.06.2021

## 6. References

- [1] S. Aghajanian, H. Nieminen, A. Laari, T. Koiranen, Integration of a calcium carbonate crystallization process and membrane contactor-based CO<sub>2</sub> capture, *Sep. Purif. Technol.* (2021) 119043. doi:10.1016/j.seppur.2021.119043.
- [2] M.A. McDonald, H. Salami, P.R. Harris, C.E. Lagerman, X. Yang, A.S. Bommarius, M.A. Grover, R.W. Rousseau, Reactive crystallization: a review, *React. Chem. Eng.* (2021). doi:10.1039/D0RE00272K.
- [3] M. Barrett, D. O'Grady, E. Casey, B. Glennon, The role of meso-mixing in anti-solvent crystallization processes, *Chem. Eng. Sci.* 66 (2011) 2523–2534. doi:10.1016/j.ces.2011.02.042.
- [4] D.V. Gradov, G. González, M. Vauhkonen, A. Laari, T. Koiranen, Experimental investigation of reagent feeding point location in a semi-batch precipitation process, *Chem. Eng. Sci.* 190 (2018) 361–369. doi:10.1016/j.ces.2018.06.042.
- [5] I. Ostergaard, B. Szilagy, Z.K. Nagy, H.L. de Diego, H. Qu, Polymorphic Control and Scale-up Strategy for Crystallization from a Ternary Antisolvent System by Supersaturation Control, *Cryst. Growth Des.* 20 (2020) 1337–1346. doi:10.1021/acs.cgd.9b01623.
- [6] T. Zhang, B. Nagy, B. Szilágyi, J. Gong, Z.K. Nagy, Simulation and experimental investigation of a novel supersaturation feedback control strategy for cooling crystallization in semi-batch implementation, *Chem. Eng. Sci.* 225 (2020) 115807. doi:10.1016/j.ces.2020.115807.
- [7] F. Caccavale, M. Iamarino, F. Pierri, V. Tufano, Control and monitoring of chemical batch reactors, Springer London, London, 2011. doi:10.1007/978-0-85729-195-0.
- [8] M. Kano, M. Ogawa, The state of the art in chemical process control in Japan: Good practice and questionnaire survey, *J. Process Control.* 20 (2010) 969–982. doi:10.1016/j.jprocont.2010.06.013.
- [9] M. Shamsuzzoha, S. Skogestad, The setpoint overshoot method: A simple and fast closed-loop approach for PID tuning, *J. Process Control.* 20 (2010) 1220–1234. doi:10.1016/j.jprocont.2010.08.003.
- [10] W. Hu, G. Xiao, Analytical proportional–integral (PI) controller tuning using closed-loop setpoint response, *Ind. Eng. Chem. Res.* 50 (2011) 2461–2466. doi:10.1021/ie101475n.
- [11] N. Ghadipasha, J.A. Romagnoli, S. Tronci, R. Baratti, On-line control of crystal properties in nonisothermal antisolvent crystallization, *AIChE J.* 61 (2015) 2188–2201. doi:10.1002/aic.14815.
- [12] M. Porru, L. Özkan, Simultaneous design and control of an industrial two-stage mixed suspension mixed product removal crystallizer, *J. Process Control.* 80 (2019) 60–77. doi:10.1016/j.jprocont.2019.04.011.
- [13] G. Rao, S. Aghajanian, T. Koiranen, R. Wajman, L. Jackowska-Strumillo, Process monitoring of antisolvent based crystallization in low conductivity solutions using electrical impedance spectroscopy and 2-D electrical resistance tomography, *Appl. Sci.* 10 (2020) 3903. doi:10.3390/app10113903.



<b>TOMOCON</b>				<b>GRANT AGREEMENT No.: 764902</b>	
Deliverable Title: <b>Lab-type Integrated Controller Structures for TOMOCON Demonstrations</b>					
<b>Del. Rel. No.</b>	<b>EU Del. No.</b>	<b>WP No.</b>	<b>Lead Beneficiary</b>	<b>Type</b>	<b>Date</b>
D4.3.	D14	WP4	ULIB	Report	15.06.2021

- [14] G. Rao, M.A. Sattar, R. Wajman, L. Jackowska-Strumillo, Quantitative evaluations with 2d electrical resistance tomography in the low-conductivity solutions using 3d-printed phantoms and sucrose crystal agglomerate assessments, *Sensors*. 21 (2021) 564. doi:10.3390/s21020564.
- [15] K. Cukierski and B. G. Thomas, Flow Control with Local Electromagnetic Braking in Continuous Casting of Steel Slabs, *Metallurgical and Materials Transactions B*, Vol. 39, No. 1, pp. 94–107, 2007.
- [16] R. Chaudhary, B. G. Thomas, and S. P. Vanka, Effect of Electromagnetic Ruler Braking (EMBr) on Transient Turbulent Flow in Continuous Slab Casting using Large Eddy Simulations, *Metallurgical and Materials Transactions B*, Vol. 43, No. 3, pp. 532–553, 2012.
- [17] B. G. Thomas and S. M. Cho, Overview of Electromagnetic Forces to Control Flow During Continuous Casting of Steel, *IOP Conference Series: Materials Science and Engineering*, Vol. 424, p. 012027, 2018.
- [18] S. Abouelazayem, I. Glavinić, T. Wondrak, and J. Hlava, Control of Jet Flow Angle in Continuous Casting Process using an Electromagnetic Brake, *IFAC-PapersOnLine*, Vol. 52, No. 14, pp. 88–93, 2019.
- [19] S. Abouelazayem, I. Glavinić, T. Wondrak, and J. Hlava, Flow Control Based on Feature Extraction in Continuous Casting Process, *Sensors*, Vol. 20, No. 23, p. 6880, 2020.
- [20] L. Zhang, S. Yang, K. Cai, J. Li, X. Wan, and B. G. Thomas, Investigation of Fluid Flow and Steel Cleanliness in the Continuous Casting Strand, *Metallurgical and Materials Transactions B*, Vol. 38, No. 1, pp. 63–83, 2007.

